Article:
Jamali, M., Sadabadi, M.S. and Davari, M. (2025) A set-theoretic adaptive current control design for grid-following inverter-based resources to tackle practically non-ideal control inputs. IEEE Transactions on Automation Science and Engineering. ISSN 1545-5955

https://doi.org/10.1109/tase.2024.3507616

A Set-Theoretic Adaptive Current Control Design for Grid-Following Inverter-Based Resources to Tackle Practically Non-Ideal Control Inputs

Mahmood Jamali, Mahdieh S. Sadabadi, *Senior Member, IEEE*,
and Masoud Davari*, *Senior Member, IEEE*

***Abstract*—Three-phase grid-following (GFL) inverter-based resources (IBRs) play a vital role as an interface for integrating renewable energy resources and flexible loads, such as electric vehicles, into the power grid. This paper introduces a novel set-theoretic adaptive control scheme for the primary control of three-phase GFL IBRs, designed to mitigate the impacts of uncertainties or non-ideal conditions affecting the control layer. These uncertainties will risk losing the stability and intended operation of three-phase GFL IBRs by potentially influencing the control commands transmitted to pulse width modulators. In order to address this issue, this study proposes an add-on control signal generated through an adaptive architecture to retrofit the existing (pre-designed) state feedback controller of GFL IBRs. As the name implies, this retrofit control strategy entails upgrading or modifying the existing feedback control instead of completely replacing it. The proposed control scheme is based on a set-theoretic adaptive controller design that employs generalized restricted potential functions. A notable aspect of this framework is its ability to ensure that the reference tracking error bound remains below a user-defined threshold, making it "computable" by providing the control design parameters. The stability of the closed-loop system and the approximate reference tracking performance of the proposed control scheme for GFL IBRs are validated through a theoretical analysis employing the Lyapunov theory. Simulation-based and experimental results further confirm the efficacy of the proposed GFL IBR controller.**

The work of Masoud Davari was supported in part by the Division of Electrical, Communications and Cyber Systems (ECCS) in the U.S. National Science Foundation (U.S. NSF) through the core program of Energy, Power, Control, and Networks (EPCN), ECCS-EPCN-EAGER and ECCS-EPCN Awards under Grant #2405252, Grant #1902787, and Grant #1808279; in part by the Office of International Science and Engineering (OISE) in the U.S. NSF through the program of International Research Experiences for Students (IRES), OISE-IRES Award under Grant #2152905; in part by the dSPACE company; in part by the Verivolt company; in part by the Semikron Danfoss company; in part by the Chroma ATE Inc. company; in part by the RTDS Technologies-AMETEK, Inc. company; in part by the Spitzenberger & Spies company; in part by the Professional Development Part of Masoud Davari's Discovery & Innovation Award from the 2020–2021 University Awards of Excellence at Georgia Southern University; and in part by the 2022 Impact Area Accelerator Grant funded by Georgia Southern University—where all the experiments to test the effectiveness and efficacy of the methodology proposed for inverter-based resources were conducted in the Laboratory for Advanced Power and Energy Systems (LAPES). *(*Corresponding author: Masoud Davari.)*

Mahmood Jamali is with the School of Electrical and Electronic Engineering, University of Sheffield, Sheffield S1 4DT, United Kingdom (e-mail: mahmood.jamali@sheffield.ac.uk).

Mahdieh S. Sadabadi is with the Department of Electrical and Electronic Engineering, The University of Manchester, Manchester, United Kingdom (e-mail: mahdieh.sadabadi@manchester.ac.uk).

Masoud Davari is with the Department of Electrical and Computer Engineering, Georgia Southern University (Statesboro Campus), Statesboro, GA 30460 USA (e-mail: mdavari@georgiasouthern.edu; davari@ualberta.ca).

***Note to Practitioners*—Given the strive to focus on renewables-intensive and modern power grids, inverters must exhibit enhanced intelligence and versatility to accommodate various functionalities. However, uncertainties or non-ideal conditions originating from diverse sources significantly threaten the optimal operation of inverter-based resources. These uncertainties introduce errors into the control loop of grid-following inverter-based resources, potentially compromising their stability and performance. In order to tackle this compelling challenge, this paper proposes a novel set-theoretic adaptive current control scheme for grid-following inverter-based resources using an add-on control signal. The aim is to mitigate the adverse effects of uncertainties affecting the control commands in grid-following inverter-based resources. By incorporating the additional control signals into the feedback controller, reference tracking is assured despite uncertainties. This approach offers a more cost-effective solution by enhancing the existing feedback control instead of entirely replacing it. Lyapunov stability theory provides a theoretical framework for analyzing stability and ensuring the uniform boundedness of output trajectories in grid-following inverter-based resources. Simulation and experimental results confirm the feasibility and effectiveness of the proposed approach in mitigating the uncertainties affecting the control commands.**

***Index Terms*—Set-theoretic adaptive control, three-phase grid-following (GFL) inverter-based resources (IBRs), uncertainties, vector current control.**

I. Introduction

In recent years, three-phase grid-following (GFL) inverter-based resources (IBRs) (hereinafter referred to as GFL IBRs for simplicity) have gained widespread use due to the increasing penetration of renewable generation resources and energy storage systems as well as the growing demand in electric vehicles [1]. These modern power electronic devices play a critical role as an interface between diverse energy sources and the main grid, boosting reliability, flexibility, and overall capacity in modern power grids [2].

In the grid modernization paradigm, e.g., smart grids or the grid edge, it is essential to implement an appropriate control strategy for GFL IBRs. This strategy ensures that GFL IBRs operate as close as possible to a current source and remain synchronized with the main electrical grid. The critical control objectives in the GFL IBRs are minimizing the steady-state tracking errors of the output currents injected into the grid and reducing the total harmonic distortion (THD) of the output currents of GFL IBRs. Furthermore, ensuring

the reliable, secure, and robust operation of GFL IBRs is paramount, given their susceptibility to various unforeseen uncertainties or non-ideal conditions due to internal faults, failures, and external disturbances, such as cyberattacks [3]. The impact of uncertainties in power grid operations can lead to instability and hazardous conditions, posing risks such as blackouts, equipment damage, and failures. Implementing advanced robust control methodologies remains crucial for mitigating the effects of uncertainties and ensuring the "*self-adapting*" of GFL IBRs. For a GFL IBR, the self-adapting feature refers to the ability of the inverter to adapt itself to either internal or external operational uncertainties.

Recent studies have introduced various control strategies for grid following inverters under disturbances and faults; see [4]–[9]. The authors in [4] have suggested an adaptive controller resilient against additive sensor data manipulations. In a noteworthy example, an active disturbance rejection control presented in [5] provides resilience for GFL IBRs with *LCL* filters against grid voltage variations and filter resonance. Similarly, the study in [8] presents a robust active damping method based on linear active disturbance rejection control to address filter resonance issues. Also, the study [6] designs an observer-based control strategy in the $\alpha\beta$ stationary frame for grid-tied inverters to cope with both balanced and unbalanced grid voltages. The authors in [10] have proposed an adaptive switching control approach to the primary control of grid-connected inverters specifically designed to rectify faulty signals in sensors. The proposed approach employs a sliding-mode controller to improve the robustness of the primary control in the direct-quadrature-frame (the *dq*-frame) against sensor faults. Likewise, in [11], a control methodology has been developed to diagnose and address issues arising from current sensor malfunctions within a photovoltaic array. In [12], researchers have proposed a two-degrees-of-freedom estimator-based controller designed to minimize the THD. The proposed controller aims to minimize tracking errors in inverter output voltage even in the presence of an uncertain system model. the study in [13] introduced a robust current control strategy for grid-connected inverters, with a specific emphasis on uncertain system models. However, this study does not account for any uncertainties in the control command of grid-connected inverters.

In the control literature, significant efforts have been made to design control strategies that mitigate the effects of disturbances and model uncertainties in dynamic systems. For instance, a robust current control scheme is proposed in [9], where grid impedance uncertainties are modeled as a polytope. A tube-based stochastic MPC strategy with a probabilistic tube is proposed in [14] to reject stochastic wind speed disturbances. Additionally, [15] explores robust output feedback model predictive control for constrained linear systems in the presence of bounded state and output disturbances.

The control techniques discussed thus far for GFL IBRs in the *dq*-frame generally address uncertainties in either model parameters or voltage disturbances originating from the grid. However, these control techniques may prove ineffective when faced with additive and multiplicative uncertainties in the control input channels (CICs). Emerging threats, such as cyberattacks, can cause GFL IBRs to encounter these types of uncertainties in the control layer, significantly degrading the desired closed-loop dynamical performance of GFL IBRs; see the simulation comparison presented in Section IV. A notable example of such uncertainties is discussed in [16], where an attacker manipulates control inputs by inserting false data injection and a multiplier. In general, existing control strategies for GFL IBRs assume controllers operate in ideal conditions without any uncertainties. Yet, in practical scenarios, GFL IBRs' controllers are prone to uncertainties that can undermine the reliability and performance of GFL IBRs, leading to instability [17].

These uncertainties may originate from diverse factors, including actuator bias, aging effects and malfunctions in sensors and actuators, degradation processes, modeling errors, parameter variation, adverse environmental conditions, and even deliberate interventions like cyberattacks. The recent survey paper in [18] discusses several practical cyberattack scenarios on inverter controllers. In addition, a new IEEE 1547.3-2023 [19] provides a guideline for cyber-security requirements in grid-interfaced distributed energy resources. This emphasizes the pressing need to investigate additional requirements in control strategies for smart inverters in modern power grids. To this end, control systems acting on inverters should be retrofitted to effectively tolerate or compensate for the uncertainties stated above, ensuring the robust and reliable operation of GFL IBRs.

Among various control strategies that aim to mitigate the impact of uncertainties in dynamic systems, the adaptive control strategy stands out as a powerful tool for dealing with additive and multiplicative uncertainties due to its inherent advantages, including robustness and superior transient performance [20]. Therefore, motivated by the identified gap in the existing literature, this paper proposes a novel set-theoretic adaptive control methodology for GFL IBRs subjected to uncertainties in their control systems. This set-theoretic adaptive control can ensure a performance guarantee at the pre-design phase. Set-theoretic approaches focus on ensuring that the system's states stay within predefined sets. Therefore, they can ensure that the system remains within a "safe set" or reaches a desired set of states [21]. This capability makes them useful in safety-critical systems, where maintaining operations within safe bounds is paramount. Indeed, the critical feature of the proposed control scheme is that it allows the tracking error bound to remain below a predetermined, user-defined bound (threshold). Since this bound is user-defined, this approach is more practical as it does not rely on unknown parameters.

Consequently, designers are able to deploy the proposed control scheme to establish guaranteed performance with a tracking error characterized by a user-defined bound at the pre-design stage. Therefore, this bound is "computable" using the given adaptive control design parameters. This set-theoretic approach significantly differs from standard model reference adaptive control methods, such as the one presented in [22], which can be conservative and have error bounds that rely on unknown parameters, thus failing to provide practical and strict performance guarantees. Another essential feature of the proposed control scheme is that it involves upgrading/modifying

the existing current feedback control rather than completely replacing it, as the name suggests. This matter is notably essential from the practical point of view, as this approach can be more cost-effective than installing an entirely new control system [23].

As discussed, uncertainties in CICs in GFL IBRs can compromise the accuracy of control commands applied to modulation signals. Any inaccuracies or corruption of such commands could lead to erroneous switching sequences. If a GFL IBR encounters a malfunction in its CIC, its ability to function effectively will be sabotaged. Specifically, the THD of the three-phase current—a pivotal metric for assessing current tracking performance—may exceed the permissible limits. Therefore, the proposed control scheme must guarantee the accurate execution of switching and modulation processes. In order to achieve this goal, an adaptive control architecture is integrated into the conventional state feedback controller in a retrofit manner. This augmentation is implemented to improve robustness and ensure stability in the face of uncertainties affecting CICs. To the best of the authors' knowledge, the ability to mitigate such uncertainties in the primary control of GFL IBRs has not been discussed in the literature. Note that the emphasis in this paper remains on the primary control stage, which is responsible for controlling and regulating the output currents (also referred to as zero-level or device-level control) [10], [24]. The main contributions of this paper are as follows.

1) It presents a novel vector current control scheme tailored for the primary control in GFL IBRs. This scheme stands out by integrating an adaptive structure, ensuring precise pulse modulation and switching. Moreover, it addresses the challenge of reference tracking in the presence of additive and multiplicative uncertainties in the current controller layer of GFL IBRs.
2) It devises a control framework to bolster the robust performance of GFL IBRs and establishes a reliable and self-adapting operation despite the additive and multiplicative uncertainties in their control systems. Notably, incorporating a retrofit command enables the output current trajectories to closely track the setpoint values—thereby ensuring that the error remains within a user-defined boundary determined by control design parameters.
3) It demonstrates that the proposed current controller guarantees the uniform ultimate boundedness of the output tracking errors of GFL IBR. This accomplishment is proven through a rigorous stability analysis grounded in Lyapunov theory and generalized barrier Lyapunov functions.

The superiority of the proposed vector current control scheme is confirmed through comparative MATLAB simulation results. Experimental results further validate and complement the findings obtained from the simulations.

The remaining sections of the paper are organized as follows. Section II presents the state-space representation of GFL IBRs utilizing the *LCL* filter and states the research problem addressed in this paper. Section III elaborates on the proposed adaptive current control framework and stability analysis. Section IV covers simulation and experimental verification. Finally, Section V concludes the paper.

Notation. The notation employed in this paper follows standard practice. $\mathbb{R}_+$ denotes the set of positive numbers, $\mathbb{R}^n$ represents real column vectors with a length of n, and $\mathbb{R}^{n\times m}$ implies the set of $n \times m$ real matrices. The notation $(.)^T$ and $(.)^{-1}$ denotes the transpose and inverse operators for matrices, respectively. $\|.\|_2$ signifies the standard 2-norm. Additionally, $\|x\|_P \triangleq \sqrt{x^T P x}$ represents the weighted Euclidean norm of $x \in \mathbb{R}^n$ with the matrix $P \in \mathbb{R}^{n\times n}$. The trace operator is denoted as tr(.). $\mathbf{0}_{n\times m}$ and $\mathbf{I}_{n\times n}$ are $n \times m$ matrix of zeros and $n \times n$ identity matrix, respectively.

II. Modelling and Problem Formulation

This section presents a dynamic modeling framework of GFL IBRs and uncertainties affecting their control system and proposes the research problem this paper aims to address.

A. Dynamical Model of GFL IBRs

Consider a GFL IBR interfaced with the main grid by an *LCL* filter, as depicted in Fig. 1. The dynamic model of such a system can be derived using Kirchhoff's circuit laws as follows.

$$\frac{\mathrm{d}i_1}{\mathrm{dt}} = \frac{1}{L_{f1}}\left(-(R_{f1}+R_f)i_1 + R_f i_2 - v_g + v_i\right) \tag{1a}$$

$$\frac{\mathrm{d}i_2}{\mathrm{dt}} = \frac{1}{L_{f2}}\left(-R_f i_1 - (R_{f2}+R_f)i_2 + v_g - v_i\right) \tag{1b}$$

$$\frac{\mathrm{d}v_{cf}}{\mathrm{dt}} = \frac{1}{C_f}(i_1 - i_2) \tag{1c}$$

where L_{f_1}/R_{f_1} is the inductance/resistance corresponding to the IBR side of the *LCL* filter; L_{f_2}/R_{f_2} is the inductance/resistance corresponding to the grid side of the *LCL* filter; C_f is the shunt capacitance of the *LCL* filter; R_f is the damping resistor; i_1 and i_2 are the inverter current and grid current; v_i and v_g are the inverter voltage (input) and grid voltage, respectively.

The mathematical model for GFL IBRs utilizing an *LCL* filter in the *dq*-frame can be represented in the state-space form by the following equations.

$$\dot{x} = A_g x + B_g u + B_v d \tag{2a}$$

$$y = C_g x \tag{2b}$$

where $x = [i_{1d} \;\; i_{1q} \;\; v_{cfd} \;\; v_{cfq} \;\; i_{2d} \;\; i_{2q}]^T \in \mathbb{R}^6$ represents the state vector, $u = [m_d \;\; m_q]^T \in \mathbb{R}^2$ denotes the input vector, $y = [i_{2d} \;\; i_{2q}]^T \in \mathbb{R}^2$ is the output vector, and the grid disturbance vector d is defined as $[v_{\mathrm{PCC}_d} \;\; v_{\mathrm{PCC}_q}]^T$. Let us define $R_{t_1} \triangleq R_{f_1} + R_f$ and $R_{t_2} \triangleq R_{f_2} + R_f$. Then, the state matrices are described as follows.

$$A_g = \begin{bmatrix} -\frac{R_{t_1}}{L_{f_1}} & \omega & -\frac{1}{L_{f_1}} & 0 & \frac{R_f}{L_{f_1}} & 0 \\ -\omega & \frac{R_{t_1}}{L_{f_1}} & 0 & -\frac{1}{L_{f_1}} & 0 & \frac{R_f}{L_{f_1}} \\ \frac{1}{C_f} & 0 & 0 & \omega & -\frac{1}{C_f} & 0 \\ 0 & \frac{1}{C_f} & -\omega & 0 & 0 & -\frac{1}{C_f} \\ \frac{R_f}{L_{f_2}} & 0 & \frac{1}{L_{f_2}} & 0 & -\frac{R_{t_2}}{L_{f_2}} & \omega \\ 0 & \frac{R_f}{L_{f_1}} & 0 & \frac{1}{L_{f_2}} & -\omega & -\frac{R_{t_2}}{L_{f_2}} \end{bmatrix} \tag{3a}$$

$$B_g = \begin{bmatrix} \frac{1}{L_{f_1}} & 0 \\ 0 & \frac{1}{L_{f_1}} \\ 0 & 0 \\ 0 & 0 \\ 0 & 0 \\ 0 & 0 \end{bmatrix}, \; B_v = \begin{bmatrix} 0 & 0 \\ 0 & 0 \\ 0 & 0 \\ 0 & 0 \\ \frac{1}{L_{f_2}} & 0 \\ 0 & \frac{1}{L_{f_2}} \end{bmatrix} \tag{3b}$$

$$C_g = \begin{bmatrix} 0 & 0 & 0 & 0 & 1 & 0 \\ 0 & 0 & 0 & 0 & 0 & 1 \end{bmatrix} \tag{3c}$$

Referring to Fig. 1, i_{d1} and i_{q1} represent the *dq*-frame components of the inverter current phasor $\overrightarrow{i_1}$, which imply i_{1a}, i_{1b}, and i_{1c}; i_{d2} and i_{q2} represent the *dq*-frame components of current phasor $\overrightarrow{i_2}$, which imply i_{2a}, i_{2b}, and i_{2c}; v_{cfd} and v_{cfq} are the *dq*-frame components of RC-filter voltage; v_{PCC_d} and v_{PCC_q} are the *dq*-frame components of $\overrightarrow{v}_{\text{PCC}}$, which depicts the point of common coupling (PCC) voltages, including v_{PCC_a}, v_{PCC_b}, and v_{PCC_c}; m_d and m_q stand for the modulation indices of the switching for GFL IBR in the *dq*-frame. P_{PCC} and Q_{PCC} represent the values for the active power and reactive power injected into the PCC, respectively.

The control input u described in (2) is designed to ensure stability and achieve rapid and smooth current reference tracking performance, as outlined by IEEE Std 1547.P10-2018 [25]. Specifically, one of the main control objectives in GFL IBRs is to maintain i_{2d} tracking $i_{\text{2d-ref}}$ and i_{2q} tracking $i_{\text{2q-ref}}$ at steady state. Here, $i_{\text{2d-ref}}$ and $i_{\text{2q-ref}}$ are the setpoints of i_{2d} and i_{2q}, respectively. Note that in the operation of a GFL IBR using the current-controlled technique and pulse width modulation (PWM), the setpoint signals ($i_{\text{2d-ref}}$ and $i_{\text{2q-ref}}$) are determined by higher-level control layers [9].

B. Uncertainty Modeling in GFL IBRs' Current Control Units

The uncertainties affecting GFL IBRs' current control systems can considerably degrade the attainable closed-loop dynamical system performance in achieving offset-free current tracking. These uncertainties may arise from various factors, including bias, aging, degradation, temperature, humidity, faults, and even cyberattacks [18], [26], [27]. Here, a general case of additive-multiplicative uncertainties in the current controller of GFL IBRs is considered. Such uncertainties are modeled as follows.

$$\tilde{u} = \Delta(u + \delta_g(t)) \tag{4}$$

where $\Delta \in \mathbb{R}^{2\times 2}$ represents a time-invariant multiplicative diagonal matrix, $\delta_g(t) \in \mathbb{R}^2$ denotes a time-varying additive vector influencing modulation indices in the primary control of GFL IBRs, and $\tilde{u}$ is the control signal applied to modulation signals. The following provides further details about the practicality of the uncertainty model in (4) are provided.

- Additive term $\delta_g(t)$ models several sources of uncertainties in the current controller—including bias, false data injection attacks on CICs, and controller-firmware update modification or insider attacks [18].
- Multiplicative term Δ, referred to as control effectiveness, models modeling errors, parameter variation [28], and different types of cyberattacks on the current control systems of GFL IBRs [18]. This term, for example, covers (i) sparse multiplicative attacks on control signals, where a malicious attacker manipulates the control input u by inserting a multiplier [16], [29] and (ii) malicious control setting attacks, where the control parameters can be compromised via edit parameters or parameter file updates by a malicious grid operator in the control server of IBRs or a malicious smart inverter portal user [18].

This paper makes the following assumption on the uncertainty model in (4).

Assumption 1. This paper assumes that the multiplicative uncertainty in CICs in (4) is *unknown* and *time-invariant*. Furthermore, the additive uncertainty $\delta_g(t)$ is assumed to *unknown* and *bounded*, i.e., $\|\delta_g(t)\| < \delta_1$, and has a bounded rate of change over time, i.e., $\|\dot{\delta}_g(t)\| < \delta_2$, where the upper bounds $\delta_1 \in \mathbb{R}$ and $\delta_2 \in \mathbb{R}$ are unknown to the control designer.

Remark 1. *This paper establishes a specific assumption regarding uncertainties in the control input of GFL IBRs. However, this assumption is realistic and not restrictive. The research does not consider unbounded uncertainties, as they are impractical for physical and operational realities. Therefore, the assumption of the boundedness of the additive uncertainty term in* (4) *is grounded in reality. It is worth noting that Assumption 1 is made without loss of generality, as even in the worst-case scenario of unbounded actuator uncertainty, practical limitations like actuator amplitude saturation naturally result in bounded behavior.*

The multiplicative uncertainty in control inputs is usually modeled as a constant scaling and remains relatively constant over time. Although it may vary over the long term, it can be reasonably approximated as time-invariant. The uncertainties affecting the current control commands in (4) can lead to data corruption and errors during the switching and modulation process. Ultimately, this disruption might prevent GFL IBRs from achieving optimal performance as intended and might lead to instability issues; see the motivation example in Subsection II-C.

C. A Motivation Example: Shortcomings of the Conventional Control Strategy for GFL IBRs

In order to achieve the *dq*-frame current reference tracking in *LCL*-filter-based GFL IBRs, a state feedback controller with an integrator is designed for the control loop system. Afterward, the control input is represented as follows.

$$\begin{aligned} u &= -K_g x - K_a x_a, \\ \dot{x}_a &= -y + r \end{aligned} \tag{5}$$

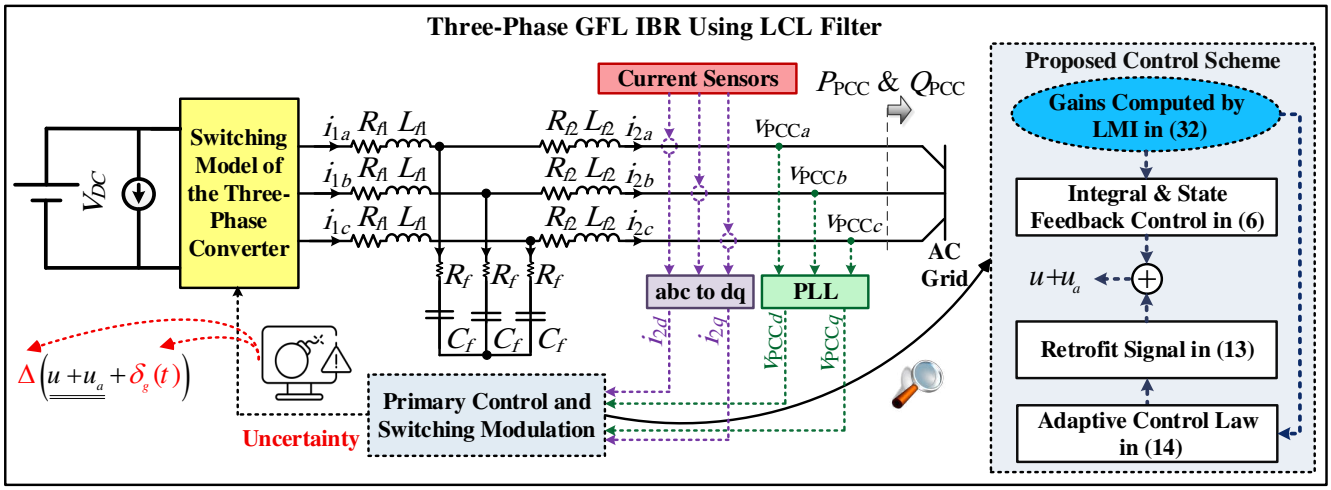

Fig. 1. Comprehensive block diagram of an *LCL*-filter-based GFL IBR employing voltage-source converter technology under multiplicative (Δ) and additive ($\delta_g(t)$) uncertainties manipulating the control input u transmitted to pulse width modulators, along with the structure of the proposed control scheme. This figure illustrates that the state feedback controller is designed based on the GFL IBR's states using the off-line linear matrix inequality (LMI) in (32). The calculated matrices K and P are applied to both the main controller (6) and the adaptive control law (14). The retrofit signal u_a introduced (13) is then updated through this adaptive structure to build up the main control command u in the primary control layer of GFL IBRs, mitigating the impacts of uncertainties acting on the control layer.

where $x_a \in \mathbb{R}^2$ denotes the integrator state, $K_g \in \mathbb{R}^{2\times 6}$ represents the feedback matrix, $K_a \in \mathbb{R}^{2\times 2}$ is the integrator gain matrix, and $r \in \mathbb{R}^2$ stands for the current setpoints vector. The control strategy in (5), which involves various methods for determining optimal parameter designs, has been widely proposed in the literature, as seen in [9], [30], [31], and references therein. Given the dynamics of a GFL IBR unit in (2), the conventional current controller in (5), and the uncertainty model in (4), the closed-loop GFL IBR system can be formulated as

$$\dot{x} = A_g x + B_g \Delta \left(-K_g x - K_a x_a + \delta_g(t)\right) + B_v d, \quad (6a)$$

$$\dot{x}_a = -y + r, \quad (6b)$$

$$y = C_g x. \quad (6c)$$

In the conventional current control design approach, the control gains in the above closed-loop dynamics are designed so that the closed-loop state matrix, as shown below, is Hurwitz, i.e., all eigenvalues of A_r are located in the left half complex plane.

$$A_r \triangleq \begin{bmatrix} A_g - B_g K_g & -B_g K_a \\ -C_g & \mathbf{0}_{2\times 2} \end{bmatrix}. \quad (7)$$

However, as modeled in (6), the closed-loop state matrix in the presence of uncertainties in CICs is presented as

$$\tilde{A}_r \triangleq \begin{bmatrix} A_g - B_g \Delta K_g & -B_g \Delta K_a \\ -C_g & \mathbf{0}_{2\times 2} \end{bmatrix}. \quad (8)$$

Obviously, the stability of A_r in (7) does not imply the stability of $\tilde{A}_r$ for $\Delta \neq \mathbf{I}_{2\times 2}$. In order to provide further details and illustrate the limitations of the conventional state feedback control strategy, a scenario where only the multiplicative uncertainty impacts the control input u is considered. For simplicity, this paper assumes that both diagonal elements of Δ are identical. Fig. 2 demonstrates how the maximum real-part of the eigenvalues of the closed-loop state matrix in (8) fluctuates with variations in the diagonal elements of Δ.

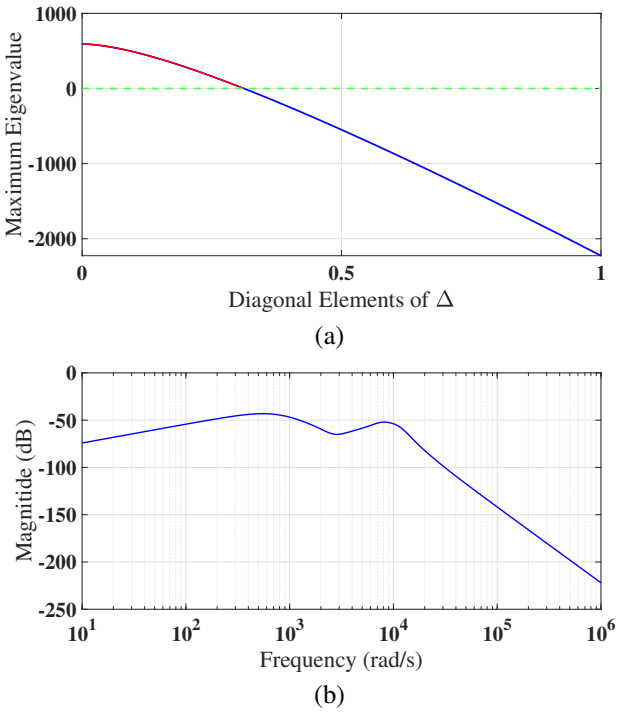

Fig. 2. (a): Maximum real-part of the eigenvalues of the closed-loop state matrix versus Δ values. The red line indicates the values of Δ that render the system unstable, (b): Magnitude Bode diagram of the closed-loop GFL IBR system from the first element of output y to the first element of input $\delta_g(t)$.

This graph utilizes the parameters outlined in Section IV. As depicted in Fig. 2, the closed-loop GFL IBR system becomes unstable for some values of Δ.

In order to assess the impact of the additive uncertainty term δ_g in (6a), let us assume that $\Delta = \mathbf{I}_2$. As the closed-loop system described in equation (6) is multi-input multi-

output, for the sake of simplicity, this paper assesses the magnitude of the Bode diagram of the closed-loop control system from the first output to the first input. It can be seen very high magnitudes at some frequencies in the Bode plot in Fig. 2, which indicates that the closed-loop GFL IBR system amplifies the additive uncertainty signal at those frequencies significantly. This matter means that such uncertainties at some frequencies can cause the GFL IBR system to resonate or amplify, leading to undesirable behavior in current signals injected into the grid.

D. Problem Statement

In order to supply the demanded power, a current controller for GFL IBRs must be designed to track the setpoints determined by the desired active power and reactive power. The scenarios mentioned in Subsection II-C highlight that the conventional feedback control scheme in (5) is inadequate and unable to accomplish current tracking performance in the presence of additive and multiplicative uncertainties in control inputs. In order to enhance the reliable operation of GFL IBRs in the face of such uncertainties, the conventional current controller in (5) should be retrofitted so that a self-adapting feature is added to the GFL IBRs. This action enhances the ability of a GFL IBR to adapt itself to operational uncertainties.

Now, the following states the research problem this paper seeks to address.

Problem 1. *Given the dynamics of a GFL IBR in* (2) *and the uncertainty model in* (4)*, the problem formulation is formed in this paper to address how to retrofit the current controller in* (5) *so that the following objectives are satisfied despite the presence of such uncertainties.*

1) *The closed-loop stability is guaranteed.*
2) *The approximate current reference tracking performance is achieved, i.e.,* $\lim_{t\to\infty}\|y(t)-r\|_2 \leq \epsilon_I$*, where* ϵ_I *is a small non-negative scalar. Therefore, the output currents of GFL IBRs,* i_{2d} *and* i_{2q}*, can track* $i_{2d\text{-}ref}$ *and* $i_{2q\text{-}ref}$*, respectively, at steady state with a predetermined, user-defined upper bound* ϵ_I*.*

The solution to Problem 1 aims to estimate the uncertainties introduced in (4) in the current controller of GFL IBRs and mitigate their effects by adding a retrofit (corrective) signal to the control input u. This signal is generated and updated by the designed uncertainty estimator, which (14) describes. The following section proposes an adaptive control scheme relying on a retrofit signal.

III. Set-theoretic Adaptive Control Scheme

This section presents an adaptive current control scheme that relies on a set-theoretic approach and incorporates a retrofit signal to improve the performance of GFL IBRs in the presence of uncertainties discussed in Subsection II-B. The proposed control scheme aims to provide a solution to Problem 1 stated in Subsection II-D.

A. Proposed Adaptive Current Control Framework

This paper proposes an adaptive current control framework for GFL IBRs. Before presenting the adaptive current control framework, let us define the augmented state vector and the augmented feedback control gain as $x_{aug} \triangleq [x^T \quad x_a^T]^T \in \mathbb{R}^8$ and $K \triangleq [K_g \quad K_a] \in \mathbb{R}^{2\times 8}$. Next, the augmented form of the system in (6) can be rewritten in a compact form as follows.

$$\begin{aligned} \dot{x}_{aug} &= Ax_{aug} + B\Delta\left(-Kx_{aug} + \delta_g(t)\right) + B_r r + B_{va} d, \\ y &= Cx_{aug}, \end{aligned} \tag{9}$$

where

$$\begin{aligned} A &\triangleq \begin{bmatrix} A_g & \mathbf{0}_{6\times 2} \\ -C_g & \mathbf{0}_{2\times 2} \end{bmatrix}, \\ B &\triangleq \begin{bmatrix} B_g^T & \mathbf{0}_{2\times 2} \end{bmatrix}^T,\ B_{va} \triangleq \begin{bmatrix} B_v^T & \mathbf{0}_{2\times 2} \end{bmatrix}^T, \\ B_r &\triangleq \begin{bmatrix} \mathbf{0}_{6\times 2}^T & \mathbf{I}_{2\times 2} \end{bmatrix}^T,\ C \triangleq \begin{bmatrix} C_g & \mathbf{0}_{2\times 2} \end{bmatrix}. \end{aligned} \tag{10}$$

Adding and subtracting BKx_{aug} to and from (9) yields

$$\dot{x}_{aug} = A_r x_{aug} + B\Delta\delta_a^T(t) z(x_{aug}) + B_r r + B_{va} d, \tag{11}$$

where A_r is given by (7), $\delta_a(t) \triangleq [\delta_g(t) \quad (\Delta^{-1} - \mathbf{I}_{2\times 2})K]^T \in \mathbb{R}^{2\times 9}$ is an aggregated uncertainty matrix; $z(x_{aug}) \triangleq [1 \quad x_{aug}^T]^T \in \mathbb{R}^9$. Note that in (11), the term $\Delta\delta_a^T(t)z(x_{aug})$, where $\Delta\delta_a^T(t)$ is unknown, linearly parameterizes the uncertainty in CICs.

Afterward, a closed-loop reference model for GFL IBRs given is considered and described by

$$\begin{aligned} \dot{x}_r &= A_r x_r + B_r r + B_{va} d, \\ y_r &= C x_r \end{aligned} \tag{12}$$

where x_r is the reference state vector, and y_r is the reference output vector for GFL IBRs. Due to the integral term in the conventional control scheme and stability of A_r, one can show that $\lim_{t\to\infty} y_r(t) = r$.

Here, the main objective is to design a retrofit signal for the current control law. This retrofit signal ensures that the error between the state of the uncertain dynamical GFL IBR system, described by (11), and the state of the reference model, described by (12), remains uniformly bounded. In the next step, adding the following retrofit signal modifies the current control law.

$$u_a(t) = -\hat{\delta}_a^T(t) z(x) \tag{13}$$

where $\hat{\delta}_a(t) \in \mathbb{R}^{9\times 2}$ is an estimate of $\delta_a(t)$ and it is updated by the following adaptive control law.

$$\dot{\hat{\delta}}_a = \beta\ \text{Proj}_{\text{m}}\left(\hat{\delta}_a(t), \psi_d(\|e\|_P) z(x) e^T P B\right), \tag{14}$$

where Proj is the projection operator defined in Appendix A in Section VI, $\beta \in \mathbb{R}_+$ is the adaptation gain, referred to as learning rate, $e \triangleq x_{aug} - x_r$ is the state of the error system, $\psi_d(\|e\|_P)$ can be obtained using (38) in Appendix B, and $P \in \mathbb{R}^{8\times 8}$ is a positive-definite solution of the following Lyapunov equation.

$$A_r^T P + P^T A_r + R = 0 \tag{15}$$

where $R \in \mathbb{R}^{8\times 8}$ is a positive-definite matrix.

Remark 2. *The projection operator in* (14) *is employed to provide a bounded estimation* $\hat{\delta}_a$.

Remark 3. *As* A_r *is Hurwitz, according to converse Lyapunov theory [32], for a given positive-definite matrix* R*, there is a unique positive-definite matrix* P *satisfying* (15)*.*

The following discusses the stability of the closed-loop GFL IBR with the adaptive control scheme in (13) and (14).

B. Closed-Loop Stability Analysis

This subsection is dedicated to proving the stability of GFL IBRs equipped with the proposed control scheme and demonstrating the achievement of the objectives stated in II-D. For the next theorem, which presents the main theoretical result of this paper, let us define $\tilde{\delta}_a(t) \triangleq \hat{\delta}_a(t) - \delta_a(t)$. Then, deploying (11)-(14), the error dynamics are described by

$$\dot{e} = A_r e - B\Delta\tilde{\delta}_a^T(t)z(x). \tag{16a}$$

$$\dot{\tilde{\delta}}_a = \beta\ \text{Proj}_{\text{m}}\left(\hat{\delta}_a(t), \psi_d(\|e\|_P)z(x)e^T PB\right) - \dot{\delta}_a(t). \tag{16b}$$

The following theorem discusses the boundeness of $(e, \tilde{\delta}_a)$.

Theorem 1. *Consider the GFL IBR system described by* (2) *under both multiplicative and additive uncertainties in CICs, as per Assumption 1. Utilizing the reference model provided in* (12)*, along with the feedback control law presented in* (6) *and the proposed adaptive control law in* (13) *and* (14)*, the error dynamics of* e *and* $\tilde{\delta}_a(t)$ *in* (16) *remain bounded for all initial conditions* $(e(0), \tilde{\delta}_a(0))$*. Furthermore, if* $\|e(0)\|_P < \epsilon_P$*, then the bound on the error satisfies a-priori given, user-defined worst-case performance* $\|e(t)\|_P < \epsilon_P$*,* $\forall t \geq 0$*. Moreover, in the case where the additive uncertainty is time-invariant, i.e.,* $\delta_g(t) = \delta$*, then* $\lim_{t\to\infty} e = \mathbf{0}_{8\times 1}$.

Proof. In order to demonstrate the boundedness of the error dynamics in (16), the Lyapunov candidate of $V : \mathcal{D}_\epsilon \times \mathbb{R}^{9\times 2} \to \mathbb{R}_+$ with $\mathcal{D}_\epsilon = \{\|e\|_P : \|e\|_P < \epsilon_P\}$ is chosen.

$$V(e, \tilde{\delta}_a) = \psi(\|e\|_P) + \beta^{-1}\text{tr}\left((\tilde{\delta}_a\Delta^{\frac{1}{2}})^T(\tilde{\delta}_a\Delta^{\frac{1}{2}})\right) \tag{17}$$

where P is the solution of the Lyapunov equation in (15). It is clear that $V(0,0) = 0$, and $V(e, \tilde{\delta}_a) > 0$ for all $(e, \tilde{\delta}_a) \neq (0,0)$. Considering the cyclic property of the trace operator [33], the time derivative of (17) is derived as follows.

$$\dot{V}(e, \tilde{\delta}_a) = \frac{\mathrm{d}\psi(\|e\|_P)}{\mathrm{d}\|e\|_P^2}\frac{\mathrm{d}\|e\|_P^2}{\mathrm{d}t} + 2\beta^{-1}\text{tr}\left(\tilde{\delta}_a^T\dot{\tilde{\delta}}_a\Delta\right). \tag{18}$$

From the definition of the weighted Euclidean norm and the derivative of the generalized barrier Lyapunov function in (38) and by considering the weight estimation error dynamics in (16b), one concludes that

$$\dot{V}(e, \tilde{\delta}_a) = 2\psi_d(\|e\|_P)e^T(t)P\dot{e}(t) + 2\text{tr}\left(\tilde{\delta}_a^T\big(\text{Proj}_{\text{m}}(\hat{\delta}_a(t), \psi_d(\|e\|_P)z(x)e^T(t)PB) - \beta^{-1}\dot{\delta}_a(t)\big)\Delta\right). \tag{19}$$

Using (16a), one can obtain

$$\begin{aligned}\dot{V}(e, \tilde{\delta}_a) = {} & 2\psi_d(\|e\|_P)e^T(t)PA_r e \\ & - 2\psi_d(\|e\|_P)e^T(t)PB\Delta\tilde{\delta}_a^T(t)z(x) + 2\text{tr}\Big(\tilde{\delta}_a^T \\ & \times \text{Proj}_{\text{m}}\left(\hat{\delta}_a(t), \psi_d(\|e\|_P)z(x)e^T(t)PB\right)\Delta\Big) \\ & - 2\beta^{-1}\text{tr}\left(\tilde{\delta}_a^T(t)\dot{\delta}_a(t)\Delta\right).\end{aligned} \tag{20}$$

Applying the cyclic and linear mapping properties of the trace operator to (20), $\dot{V}(e, \tilde{\delta}_a)$ can be described as

$$\begin{aligned}\dot{V}(e, \tilde{\delta}_a) = {} & 2\psi_d(\|e\|_P)e^T(t)PA_r e \\ & + 2\text{tr}\Big(\tilde{\delta}_a^T\Big(- \psi_d(\|e\|_P z(x)e^T(t)PB \\ & + \text{Proj}_{\text{m}}(\hat{\delta}_a(t), \psi_d(\|e\|_P)z(x)e^T(t)PB)\Delta\Big)\Big) \\ & - 2\beta^{-1}\text{tr}\left(\tilde{\delta}_a(t)\dot{\delta}_a(t)\Delta\right).\end{aligned} \tag{21}$$

Next, given (15) and the property of the projection operator for matrices in (36), one can get the following inequality.

$$\dot{V}(e, \tilde{\delta}_a) \leq -\lambda_{min}(R)\psi_d(\|e\|_P)e^T(t)Pe + \sigma, \tag{22}$$

with $\sigma \triangleq 2\beta^{-1}\delta_{a1}\delta_{a2}\|\Delta\|_2$, where $\|\delta_a\| < \delta_{a1}$ and $\|\dot{\delta}_a\| < \delta_{a2}$. By adding and subtracting $\frac{1}{2}\alpha\psi(\|e\|_P)$ and $\frac{1}{2}\alpha\beta^{-1}\text{tr}\left(\left(\tilde{\delta}_a\Delta^{\frac{1}{2}}\right)^T\left(\tilde{\delta}_a\Delta^{\frac{1}{2}}\right)\right)$ to and from (22), one concludes that

$$\begin{aligned}\dot{V}(e, \tilde{\delta}_a) \leq {} & -\frac{1}{2}\alpha\Big(\psi(\|e\|_P) + \beta^{-1}\text{tr}\big((\tilde{\delta}_a\Delta^{\frac{1}{2}})^T(\tilde{\delta}_a\Delta^{\frac{1}{2}})\big)\Big) \\ & - \alpha\Big(\psi_d(\|e\|_P)e^T(t)Pe - \frac{1}{2}\psi(\|e\|_P)\Big) \\ & + \frac{1}{2}\alpha\beta^{-1}\text{tr}\Big(\left(\tilde{\delta}_a\Delta^{\frac{1}{2}}\right)^T\left(\tilde{\delta}_a\Delta^{\frac{1}{2}}\right)\Big) + \sigma\end{aligned} \tag{23}$$

where $\alpha = \frac{\lambda_{min}(R)}{\lambda_{max}(P)}$. By referring to (39) and (17), the following inequality is expressed.

$$\dot{V}(e, \tilde{\delta}_a) \leq -\frac{1}{2}\alpha V(e, \tilde{\delta}_a) + \gamma, \tag{24}$$

where $\gamma \triangleq \frac{1}{2}\alpha\beta^{-1}\delta_{a1}^2\|\Delta\|_2 + \sigma$. Therefore, one can obtain

$$V(e, \tilde{\delta}_a) \leq \exp(-\frac{1}{2}\alpha t) + \frac{2\gamma}{\alpha}. \tag{25}$$

As a result, $\lim_{t\to\infty}\sup\ V(e, \tilde{\delta}_a) = \frac{2\gamma}{\alpha}$. Then, according to [32], [34], the weight estimation error dynamics in (16b) remain bounded, and the error dynamics in (16a) are proven to be Lyapunov stable for all initial conditions. This matter establishes the uniform boundedness of the error trajectories of e in (16a). Given (17) and the properties of the generalized barrier Lyapunov function in (37), the following limit for the error can be obtained.

$$\psi(\|e\|_P) = \frac{\|e\|_P^2}{\epsilon_p^2 - \|e\|_P^2} \leq \frac{2\gamma}{\alpha}, \tag{26}$$

which follows by

$$\|e\|_P \leq \frac{\epsilon_P \sqrt{\frac{2\gamma}{\alpha}}}{\sqrt{\frac{2\gamma}{\alpha}+1}} \leq \epsilon_P. \tag{27}$$

In the scenario where the additive uncertainty is time-invariant, $\sigma = 0$ as $\dot{\delta}_a = 0$. In order to advance with the proof, let us define the zero-dissipation set as

$$\Lambda := \left\{(e, \tilde{\delta}_a) \in \mathcal{D}_\epsilon \times \mathbb{R}^{9\times 2} \mid \dot{V}(e, \tilde{\delta}_a) = 0\right\}, \tag{28}$$

and $\Gamma \subseteq \Lambda$, which is the largest invariant set in Λ. Thus, it implies that all solutions approach the largest invariant set Γ. As a result, in this scenario $(e, \tilde{\delta}_a) \to \Gamma = \left\{(\mathbf{0}, \mathbf{0})\right\}$ as $t \to \infty$. Consequently, based on (6a), it can be concluded that $\lim_{t\to\infty} e = \mathbf{0}_{8\times 1}$ and $\lim_{t\to\infty} y(t) = r$, which implies Lyapunov asymptotic stability. This completes the proof. ■

The results in Theorem 1 show that the proposed set-theoretic adaptive control scheme in (13) and (14) ensures the stability of GFL IBRs in the face of uncertainties in (4) (first objective in Problem 1).

C. Current Reference Tracking Performance

According to the results in Theorem 1 in (27), the Euclidean norm of the error signal between the states of uncertain GFL IBR and the states of the reference model in (12) is upper-bounded by

$$\|e(t)\|_2 \leq \frac{\epsilon_P}{\sqrt{\lambda_{min}(P)}}, \ \forall t \geq 0. \tag{29}$$

This upper bound is solely determined by the user-defined values of ϵ_P and the design matrix parameter P. As mentioned in Section I, the designer is able to determine this tracking error bound since it only relies on the control parameter in (15) and the constant design parameter in (26). In other words, since (29) does not depend on the unknown uncertainties Δ, $\delta_g(t)$, or any other unknown parameters, this error bound can be computed during the pre-design stage, ensuring desired GFL IBR performance. Due to the properties of the Euclidean norm and (29), the upper bound of the output error is obtained as follows.

$$\|y(t) - y_r(t)\|_2 \leq \frac{\epsilon_P}{\sqrt{\lambda_{min}(P)}}, \ \forall t \geq 0. \tag{30}$$

The inequality in (30) indicates that the tracking error of the output currents of GFL IBRs, i.e., $i_{2d} - i_{\text{2d-ref}}$ and $i_{2q} - i_{\text{2q-ref}}$, is less than or equal to $\epsilon_I = \frac{\epsilon_P}{\sqrt{\lambda_{min}(P)}}$ at steady state. Thus, one can conclude that

$$\lim_{t\to\infty} \|y(t) - y_r(t)\|_2 = \lim_{t\to\infty} \|y(t) - r\|_2 \leq \frac{\epsilon_P}{\sqrt{\lambda_{min}(P)}}. \tag{31}$$

As a result, the approximate current reference tracking in Problem 1 is ensured with ϵ_I (second objective in Problem 1).

Remark 4. *For the case of time-invariant additive uncertainty term δ_g, an exact current reference tracking is achieved, i.e., $\epsilon_I = 0$.*

IV. Simulations and Experiments

This section meticulously presents comparative simulations and experimental results of the proposed vector current control methodology for two distinct uncertainty cases. Both cases involve additive and multiplicative uncertainty in the control inputs of the GFL IBR. MATLAB/Simulink simulations are conducted in order to evaluate the effectiveness of the proposed control methodology. Additionally, experimental outcomes from a GFL IBR setup for both cases are presented to underscore the practicality of the proposed adaptive control methodology. Fig 1, with parameters outlined in Table I, is considered for the tests. A sinusoidal signal is employed to emulate the bounded additive uncertainty, consistent with Assumption 1. A diagonal matrix of size 2×2 is applied to CIC for the multiplicative uncertainty. The adaptation gain for the adaptive control law in (14) is selected as $\beta = 900$. In the generalized barrier Lyapunov function (37), ϵ_P is configured to 0.01. In order to compute the values of P and the state feedback matrix K, solving a LMI problem using YALMIP is required [35]. The formulation of the LMI problem with $\alpha = 1000$ is provided by

$$\begin{aligned} PA^T + AP - K^T B^T - BK + \alpha P < 0, \\ P > 0. \end{aligned} \tag{32}$$

The solution to the above sets of LMIs is (K, P).

This paper also includes simulation results comparing the conventional feedback controller with the proposed control scheme. Furthermore, it provides the results of the sliding mode controller suggested in [10] with a control structure in (33) and the robust multi-variable controller in [30] for GFL IBRs. It is noteworthy that the robust multi-variable controller is derived as a solution to the optimization problem with the cost function in (34). These results highlight the inability of the controllers mentioned earlier to achieve satisfactory performance in the presence of additive and multiplicative uncertainties. For more details on the design process of these controllers and their stability analysis, the reader is referred to the pertinent papers cited.

$$\begin{cases} u = & -K(C_g x + s) \\ s = & z - y \\ \dot{z} = & -(\hat{\beta}||x||_2 + \hat{\alpha} + k_r)\text{sign}(s) \\ \dot{\hat{\alpha}} = & \eta||s||_2 \\ \dot{\hat{\beta}} = & \gamma||s||_2||x||_2 \end{cases} \tag{33}$$

$$J = \int_0^\infty \left(e^T(t) Q^{(0)} e(t) + z_p^T(t) Q_p z_p(t) + \nu^T(t) R_\nu \nu(t)\right) dt \tag{34}$$

where $Q^{(0)}, Q_p$, and R_{nu} are the positive definite diagonal matrices. $e(t)$ represents the error signals, $z_p(t)$ is the time derivative of currents, and $\nu(t)$ is the actual control input.

A. Simulation Results

1) Case Study I: The bounded additive uncertainty signal vector for this case study is selected to be $\delta_g(t) = \begin{bmatrix} 2\sin(10t) & \sin(20t) \end{bmatrix}^T$. The multiplicative uncertainty is chosen as $\Delta = [0.35 \quad 0; 0 \quad 0.15]$. This case study assumes that

TABLE I
PARAMETERS OF THE GFL IBR EMPLOYED IN THE SIMULATIONS AND EXPERIMENTS IN SECTION IV.

Parameter	Value
L_{f_1}/R_{f_1}	5 mH/0.06 Ω
L_{f_2}/R_{f_2}	5 mH/0.06 Ω
C_f/R_f	19 μF/2.5 Ω
$V_{\mathbf{DC}}$	500 V
f_s	8.1 kHz
$V_{\mathbf{PCC_{rms}}}$	208 V
ω_o	$2\pi 60$

both uncertainties begin at $t = 1.5$ s and persist until the end of the simulation time. Fig. 3 presents the simulation results for the signals of interest, namely the *dq*-frame currents i_{2d} and i_{2q}, active power P_{PCC}, reactive power Q_{PCC}, three-phase output current $\overrightarrow{i_2}$, and harmonic spectrum of the GFL IBR's three-phase output current $\overrightarrow{i_2}$. In order to avoid redundancy, only the harmonic spectrum of one phase is presented, as the harmonic spectra of the other two phases are similar.

Initially, the desired values of the active power and reactive power dictate that both $i_{2\text{d-ref}}$ and $i_{2\text{q-ref}}$ are set to 0. The load changes occur suddenly at $t = 0.5$ s and $t = 1$ s, respectively, to reach the setpoint values. In this scenario, a voltage sag in the grid is also considered. Voltage sags are grid disturbances primarily caused by faults, resulting in a decrease in the root mean square (RMS) voltage. The voltage sags occur at $t = 1.2$ s and $t = 1.4$ s, resulting in a 10% drop in the grid voltage. As depicted in Fig. 3, the proposed adaptive current control strategy can effectively mitigate the adverse impacts of uncertainties. Furthermore, following the uncertainties, the three-phase output current signal promptly reverts to the setpoint values within a brief period—specifically, less than 0.04 s—and maintains its sinusoidal shape.

Figs. 4 and 5 illustrate the simulation outcomes for the GFL IBR equipped with the conventional state feedback controller and the sliding mode controller, respectively. As can be seen, both controllers successfully achieve current reference tracking before the occurrence of uncertainties. After the uncertainties, however, the current, active, and reactive power signals fail to track their nominal values. As a result, the state trajectories of the GFL IBR are directed toward unintended operating points. In particular, the three-phase current is unable to quickly regain its sinusoidal shape, which is a critical requirement as specified by IEEE Std 1547.P10-2018 [25]. Furthermore, the three-phase currents' THD values, key metrics for assessing current tracking performance, exceed the permissible limits set by IEEE Std 519-2014 [36].

2) Case Study II: In this case study, CIC is subjected to uncertainties represented by $\delta_g(t) = \begin{bmatrix}4\sin(100t) & 2\sin(200t)\end{bmatrix}^T$ and $\Delta = [0.4 \quad 0; 0 \quad 0.5]$; see Fig. 6. The load changes occur at times similar to those in the previous case. Likewise, the voltage sag occurs at the exact times detailed in the previous case study, resulting in a 5% drop in the grid voltage across all phases. Despite uncertainties occurring at $t = 1.5$ s in CIC, the proposed control strategy effectively maintains the stability of the GFL IBR. Furthermore, it accurately tracks the setpoint values of the current signals, thereby achieving the desired

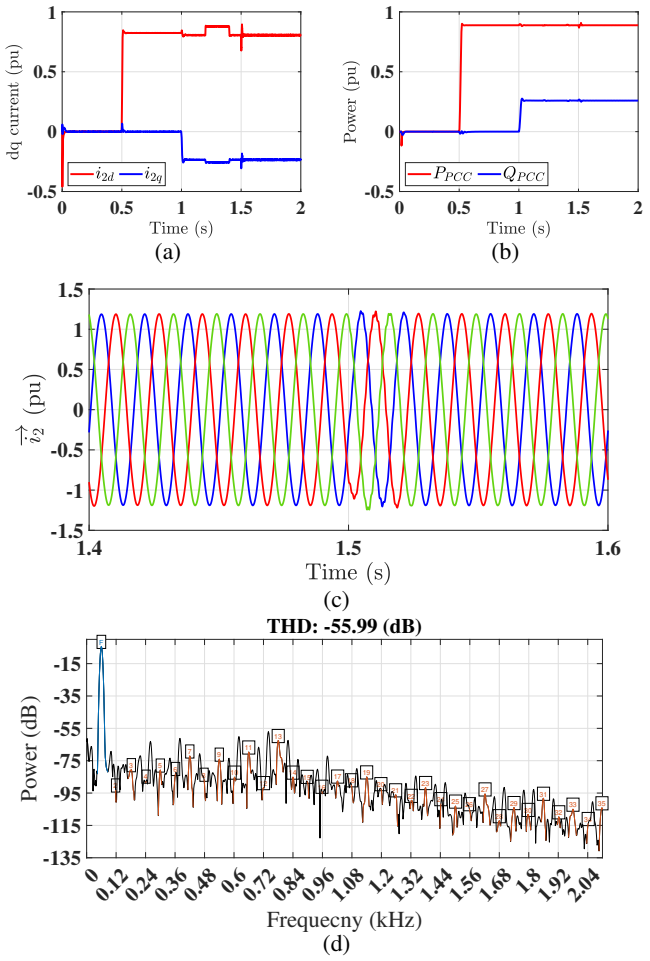

Fig. 3. Performance of the proposed adaptive control scheme for *Case Study I*: (a) *dq*-frame components of the vector of the current injected to PCC (i_{2d} and i_{2q}), (b) active power and reactive power injected to PCC (P_{PCC} and Q_{PCC}), (c) three-phase current ($\overrightarrow{i_2}$), and (d) harmonic spectrum of the three-phase current $\overrightarrow{i_2}$ with a THD of −55.99 dB or, equivalently, 0.15%.

active power and reactive power outputs of the GFL IBR.

Figs. 7 and 8 depict this case study's simulation results of the conventional state feedback current controller and the robust controller, respectively. Similar to the previous case, the GFL IBR controlled with these two controllers does not achieve setpoint current tracking after encountering both additive and multiplicative uncertainty in the control layer. Although the robust control strategy may eventually restore the *dq*-frame currents in addition to active power and reactive power, Fig. 8 demonstrates that it falls short in providing the desired and rapid performance in the presence of uncertainties compared to the proposed control scheme. Specifically, the robust controller exhibits a much slower and oscillatory transient response when the GFL IBR faces uncertainties in the control command.

3) Case Study III: This case study investigates weak-grid scenarios for simulation, where the short-circuit capacity ratio (SCCRs) or SCRs are set to 1.5. Various factors, such as grid impedance, type of grid impedance, and the phase-locked loop controller, can influence weak-grid integration [37]–[40].

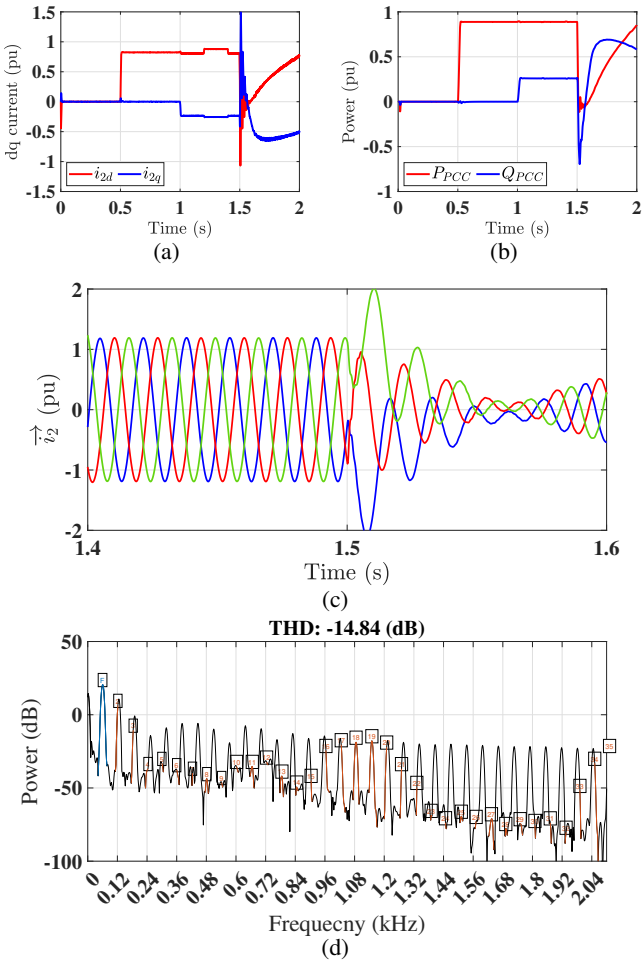

Fig. 4. Performance of the conventional state feedback current controller for *Case Study I*: (a) *dq*-frame components of the vector of the current injected to PCC (i_{2d} and i_{2q}), (b) active power and reactive power injected to PCC (P_{PCC} and Q_{PCC}), (c) three-phase current ($\overrightarrow{i_2}$), and (d) harmonic spectrum of three-phase current $\overrightarrow{i_2}$ with a THD of – 14.84 dB or, equivalently, 18.11%.

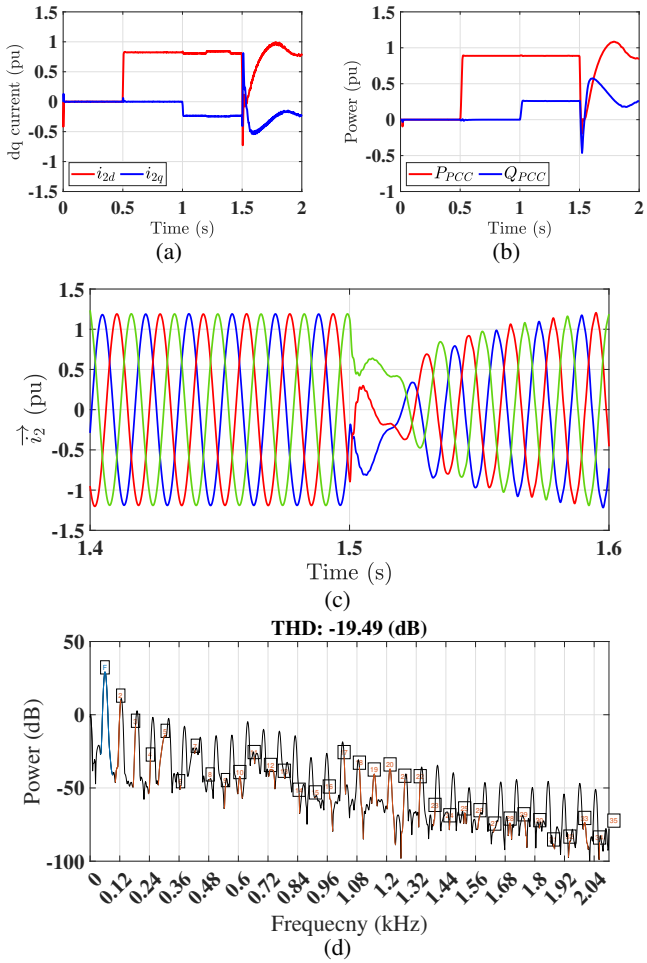

Fig. 5. Performance of the sliding mode current controller for *Case Study I*: (a) *dq*-frame components of the vector of the current injected to PCC (i_{2d} and i_{2q}), (b) active power and reactive power injected to PCC (P_{PCC} and Q_{PCC}), (c) three-phase current ($\overrightarrow{i_2}$), and (d) harmonic spectrum of three-phase current $\overrightarrow{i_2}$ with a THD of – 19.49 dB or, equivalently, 10.6%.

It is worth noting that designing a controller for weak-grid integration is beyond the scope of this paper. However, simulation results are provided to demonstrate the performance of the proposed controller when integrating GFL IBR into weak grids. The timing of the load change and the uncertainties remain consistent with *Case Study I*; however, the voltage sag scenario is not considered in this case. As shown in Fig. 9, the proposed control scheme proves effective even under weak-grid integration conditions.

B. Discussion on Simulation Results

The results presented in this section indicate that the GFL IBR equipped with the proposed control scheme demonstrates a remarkable capacity to mitigate the adverse effects of uncertainties. The three-phase and the *dq*-frame current signals quickly return to their reference values within a very short duration, precisely under approximately 0.025 seconds. The three-phase current signal effectively maintains its sinusoidal shape with a THD of less than 1%, within the range permissible by standards, e.g., IEEE Std 519-2014 [36]. The deviations in active and reactive power from their setpoints are approximately 1%, a negligible error compared to the scale of output active power and reactive power. As observed, the output signals of GFL IBR controlled by the conventional state feedback controller cannot meet the standards defined by IEEE Std 1547.P10-2018 [25], reaching an undesired operating point. While the sliding mode and robust controllers perform well in reference tracking under normal circumstances, they fail to quickly restore the signals to their nominal values when faced with additive and multiplicative uncertainties. Particularly, the excessive current changes—nearly 1 pu or higher—at the moment the uncertainties occur could cause damage to the inverter and connected devices or result in disconnection from the grid in real-world scenarios. Moreover, the peak-to-peak value of the three-phase current signals fluctuates by approximately 0.5 pu after the onset of uncertainties, impacting the proper functioning of GFL IBRs.

The THD of the three-phase current signal for one phase, following uncertainty for all strategies used in the simulations,

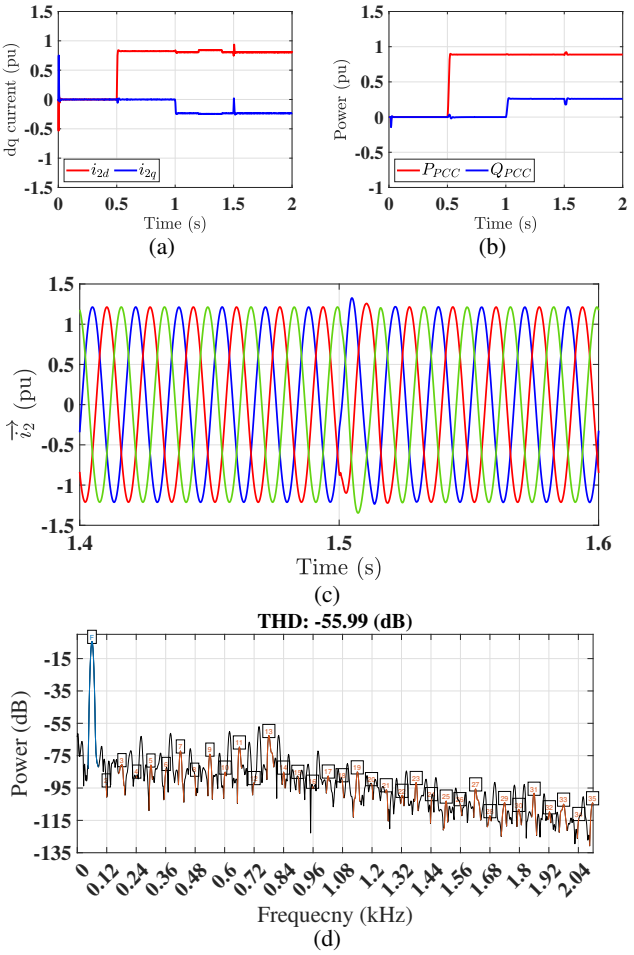

Fig. 6. Performance of the proposed adaptive control scheme for *Case Study II*: (a) *dq*-frame components of the vector of the current injected to PCC (i_{2d} and i_{2q}), (b) active power and reactive power injected to PCC (P_{PCC} and Q_{PCC}), (c) three-phase current ($\overrightarrow{i_2}$), and (d) harmonic spectrum of the three-phase current $\overrightarrow{i_2}$, with a THD of – 55.99 dB or, equivalently, 0.15%.

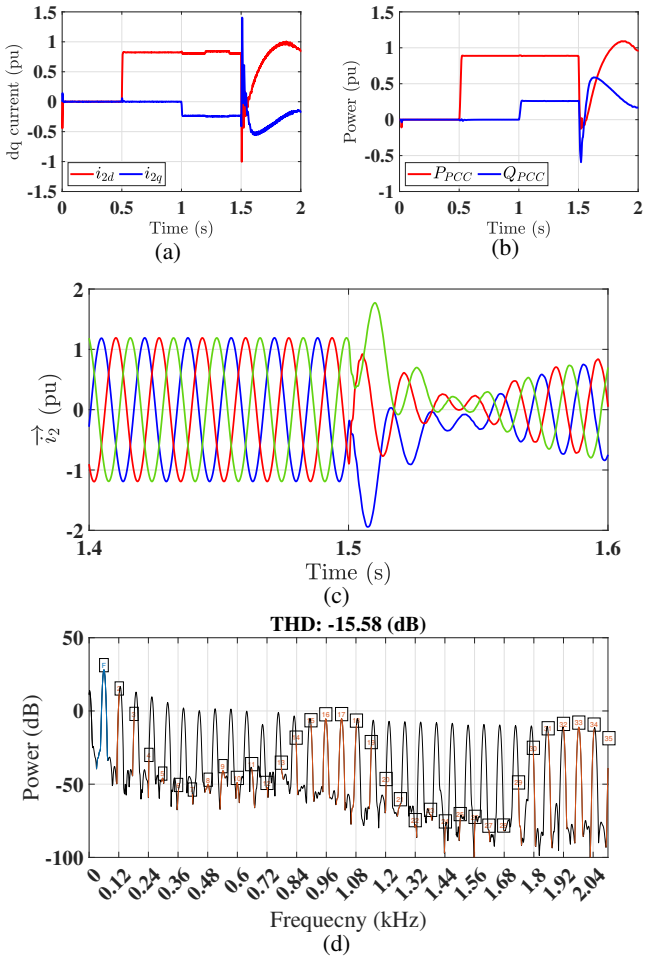

Fig. 7. Performance of the conventional state feedback current controller for *Case Study II*: (a) *dq*-frame components of the vector of the current injected to PCC (i_{2d} and i_{2q}), (b) active power and reactive power injected to PCC (P_{PCC} and Q_{PCC}), (c) three-phase current ($\overrightarrow{i_2}$), and (d) harmonic spectrum of three-phase current $\overrightarrow{i_2}$ with a THD of – 15.58 dB or, equivalently, 16.63%.

is presented in Table II. The table also provides the error metric integral time absolute error (ITAE) for the *dq*-frame currents, offering a comparative analysis of tracking errors across the methodologies discussed in this paper. These indices are crucial in ensuring precise control and robustness in various engineering applications [41]. These performance metrics assign greater penalties to errors that persist over time. A lower ITAE value indicates a more effective control strategy in promptly correcting errors. Specifically, smaller ITAE values suggest that the control strategy reduces errors early in the transient response, minimizing cumulative error and enhancing overall system performance. Conversely, higher ITAE values are associated with slower error correction, potentially due to oscillations or delays in the transient response. As shown in Table II, the smaller values of this metric for the proposed adaptive control scheme, compared to other methodologies, further validate its effectiveness in achieving accurate reference tracking.

C. Experimental Results

There are many approaches to testing the effectiveness and practicality of zero-level controls of advanced technologies to be integrated into modern power and energy systems. For example, the authors in [42] and [43] have detailed the testing based on various hardware-in-loop-based simulations—and those in [44] have applied the testing based on the rapid control prototyping (RCP) method. As there is no need for a large-scale power system in this paper, it utilizes the latter, i.e., the RCP method, to implement the proposed set-theoretic adaptive current control for GFL IBRs on a prototype unit of a GFL IBR. Fig. 10 demonstrates the test rig deployed to conduct experiments. It utilizes power modules based on insulated gate bipolar transistors, specifically the Semikron Danfoss “SKM 50 GB 123 D” intelligent power modules. The Semikron Danfoss “SKHI 21A (R)” gate drives and protection circuitry are employed to enable the functioning of the GFL IBR prototype. The Verivolt “IsoBlock I-ST-1c”/“IsoBlock V-1c” current/voltage sensors are also hooked up to the inputs of a

TABLE II
PERFORMANCE INDICES OF THE CURRENT SIGNALS FOLLOWING UNCERTAINTIES FOR THE SIMULATION SCENARIOS DISCUSSED IN SUBSECTION IV-A

Control Method (Case No.)	THD	ITAE of i_d	ITAE of i_q
Proposed Adaptive (I)	−55.99 (dB) (or 0.15 %)	0.16 (s)	0.22 (s)
Proposed Adaptive (II)	−55.99 (dB) (or 0.15 %)	0.18 (s)	0.21 (s)
Proposed Adaptive (III)	−44.53 (dB) (or 0.59 %)	0.24 (s)	0.44 (s)
State Feedback (I)	−14.84 (dB) (or 18.11 %)	11.95 (s)	12.02 (s)
State Feedback (II)	−15.58 (dB) (or 16.6 %)	5.03 (s)	7.95 (s)
Sliding Mode (I)	−19.49 (dB) (or 10.6 %)	3.19 (s)	3.98 (s)
Robust (II)	−20.43 (dB) (or 9.51 %)	1.78 (s)	2.89 (s)

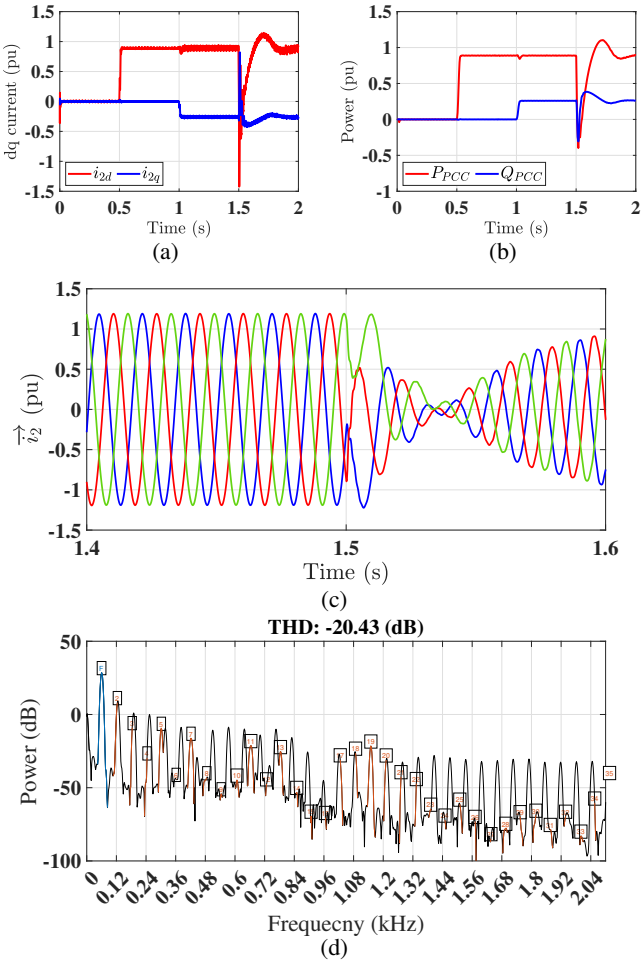

Fig. 8. Performance of the robust controller for *Case Study II*: (a) *dq*-frame components of the vector of the current injected to PCC (i_{2d} and i_{2q}), (b) active power and reactive power injected to PCC (P_{PCC} and Q_{PCC}), (c) three-phase current ($\overrightarrow{i_2}$), and (d) harmonic spectrum of three-phase current $\overrightarrow{i_2}$ with a THD of −20.43 dB or, equivalently, 9.51%.

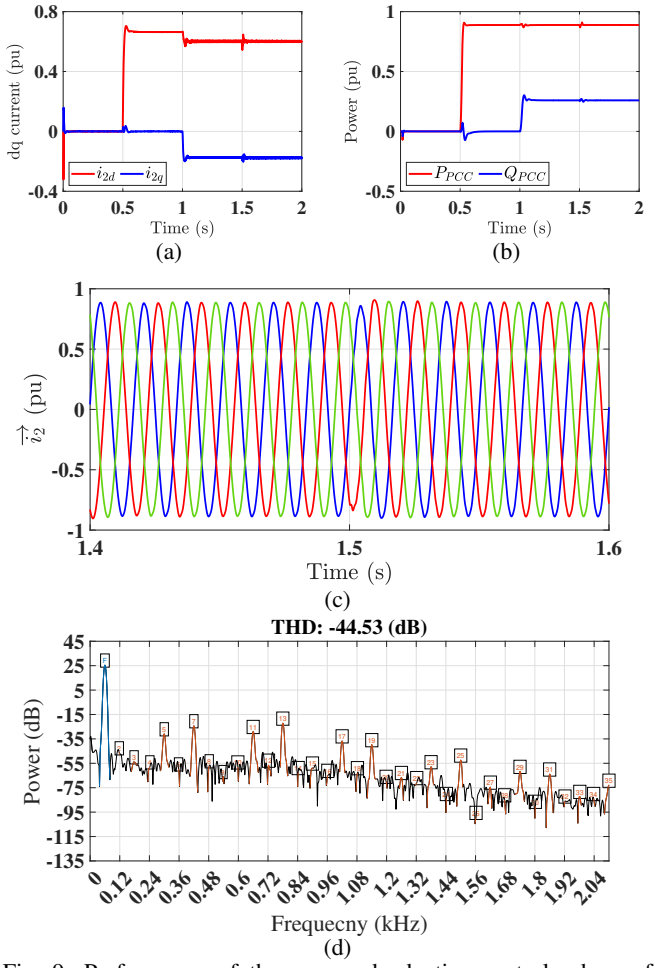

Fig. 9. Performance of the proposed adaptive control scheme for *Case Study III*: (a) *dq*-frame components of the vector of the current injected to PCC (i_{2d} and i_{2q}), (b) active power and reactive power injected to PCC (P_{PCC} and Q_{PCC}), (c) three-phase current ($\overrightarrow{i_2}$), and (d) harmonic spectrum of the three-phase current $\overrightarrow{i_2}$, with a THD of −44.53 dB or, equivalently, 0.59%.

dSPACE "MicroLabBox (MLBX)" digital real-time controller to measure currents and voltages. The dSPACE MLBX digital real-time controller's input/output channels also interface with the GFL IBR under test, as well as the measurement and drive circuitry. A field-programmable gate array generates the PWM signals; see [44] for details. Moreover, all the parameters deployed in the experiments are consistent with those in the simulations, as outlined in Table I.

Figs. 11 and 12 display the experimental results obtained for *Test Case I* and *Test Case II* of the GFL IBR shown in Fig. 1 for normal voltage. The results presented in this section clearly demonstrate the effectiveness of the proposed control scheme in mitigating the adverse effects of uncertainties. Upon the occurrence of such uncertainties, both the three-phase and the *dq*-frame current signals quickly return to their reference

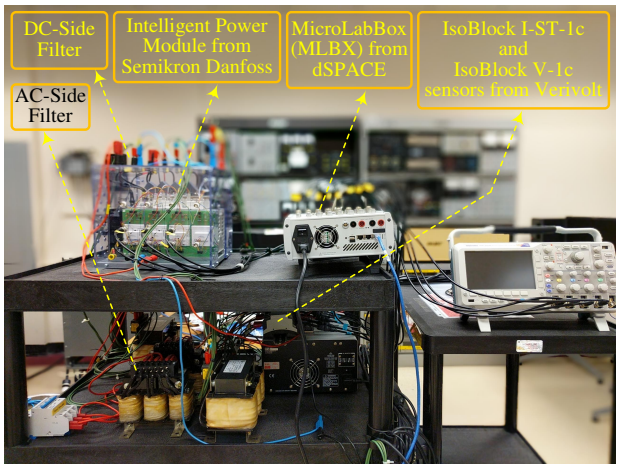

Fig. 10. Test rig deployed to carry out experiments—including the details of the GFL IBR under test—in the Laboratory for Advanced Power and Energy Systems (LAPES) at Georgia Southern Universtiy.

values within a very short timeframe. These experimental findings validate the effectiveness of the proposed control scheme based on the available resources.

D. Discussion on Experimental Results

Figs. 11 and 12 demonstrate that the *dq*-frame currents, active power, and reactive power of the GFL IBR equipped with the proposed adaptive control methodology quickly return to the reference values after encountering uncertainties in the control command. In order to calculate the THD and tracking error indices, we used data obtained from our setup, as illustrated in Fig. 11 (c) and Fig. 12 (c). These figures show that the *dq*-frame current signals closely follow the desired reference values. Additionally, the three-phase current signals maintain their sinusoidal shapes following the impact on the GFL IBR. Fig. 11 (d) and Fig. 12 (d) display their harmonic spectra in dB only for one phase. This matter is because the spectra of the other two phases are similar. The experimental results reveal that both THD values comply with the IEEE Std 519-2014 (i.e., less than 5 %) [36]. The THD values and other tracking error indices of the experimental results are presented in Table III. In addition to ITAE and THD, Table III consists of the settling time of the *dq*-frame current signals to return to the reference values after the uncertainty. Specifically, it takes less than approximately 0.3 seconds for the *dq*-frame current signals to restore to their reference values. These values for the different indices validate the efficacy of the experimental results, which are consistent with the simulation outcomes.

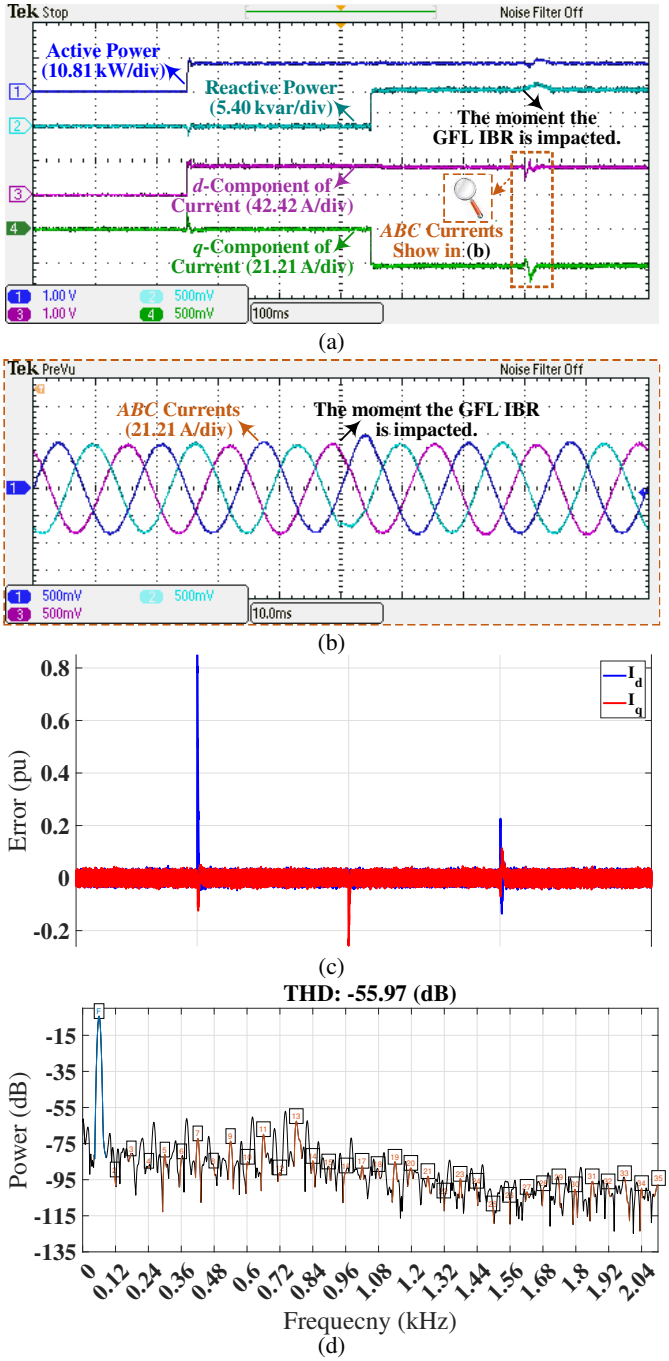

Fig. 11. Experimental results of *Case I*: (a) active and reactive power and the *dq*-frame components of the vector of the current injected to PCC (100 ms/div for the horizontal axis), (b) the *abc* currents injected to PCC (10 ms/div for the horizontal axis), (c) tracking errors of the *dq*-frame currents, and (d) harmonic spectrum of the three-phase current (for one phase) with a THD of −55.97 dB or, equivalently, 0.15%.

V. Conclusion

This paper has introduced a set-theoretic adaptive control framework for the primary control of grid-following inverter-based resources. It has mitigated the adverse effects of both additive and multiplicative uncertainty in control inputs. The proposed control methodology, designed with a retrofit control signal, has guaranteed stability and output tracking despite the existence of such uncertainties. Furthermore, the paper has conducted a rigorous stability analysis based on Lyapunov theory and generalized barrier Lyapunov functions. The effectiveness and superiority of the proposed control scheme have been validated through comparative MATLAB/Simulink simulations and experimental results.

TABLE III
PERFORMANCE INDICES OF THE CURRENT SIGNALS FOLLOWING UNCERTAINTIES FOR THE EXPERIMENTAL SCENARIOS DISCUSSED IN SUBSECTION IV-C

Case No.	Settling Time of i_d	Settling Time of i_q	THD	ITAE of i_d	ITAE of i_q
(I)	0.22 (s)	0.24 (s)	−55.97 (dB) (or 0.15%)	0.17 (s)	0.22 (s)
(II)	0.24 (s)	0.29 (s)	−55.91 (dB) (or 0.16%)	0.19 (s)	0.22 (s)

VI. APPENDICES

Appendix A: Projection Operator

Let $\Omega = \{\theta \in \mathbb{R}^n : (\theta_i^{min} \leq \theta_i \leq \theta_i^{max})_{i=1,2,...,n}\}$ denote a convex hypercube in $\mathbb{R}^n$, where θ_i^{min} and θ_i^{max} represent the minimum and maximum bounds for the i-th element of the n-dimensional vector θ. Moreover, for a sufficiently small positive constant ϵ, another hypercube is defined as $\Omega_\epsilon = \{\theta \in \mathbb{R}^n : (\theta_i^{min} + \epsilon \leq \theta_i \leq \theta_i^{max} - \epsilon)_{i=1,2,...,n}\}$, where $\Omega_\epsilon \subset \Omega$. Provided that another n-dimensional vector $\phi = \left[\phi_1, ..., \phi_i, ..., \phi_n\right]^T$, the projection operator $\text{Proj} : \mathbb{R}^n \times \mathbb{R}^n \to \mathbb{R}^n$ for $i = 1, 2, ..., n$ is defined as follows [45].

$$\text{Proj}(\theta, \epsilon) \triangleq \begin{cases} \left(\frac{\theta_i^{max} - \theta_i}{\epsilon}\right)\phi_i, & \text{if } (\theta_i > \theta_i^{max} - \epsilon \\ & \text{and } \theta_i > 0) \\ \left(\frac{\theta_i - \theta_i^{min}}{\epsilon}\right)\phi_i, & \text{if } (\theta_i < \theta_i^{min} + \epsilon \\ & \text{and } \theta_i < 0) \\ \epsilon, & \text{otherwise} \end{cases} \tag{35}$$

This definition can be further extended to matrices as $\text{Proj}_\text{m}(\Theta, \varepsilon) = (\text{Proj}(\text{col}_1(\Theta), \text{col}_1(\varepsilon)), ..., \text{Proj}(\text{col}_m(\Theta), \text{col}_m(\varepsilon))$, where $\Theta \in \mathbb{R}^{n\times m}$, $\varepsilon \in \mathbb{R}^{n\times m}$, and col_i denotes the i-th column of the respective matrix. For the matrix form of the projection operator with a given matrix Θ^*, the following inequality is satisfied [45].

$$\text{tr}\big((\Theta - \Theta^*)^T \left(\text{Proj}_\text{m}(\Theta, \varepsilon) - \varepsilon\right)\big) \leq 0. \tag{36}$$

Appendix B: Generalized Barrier Lyapunov Functions

The suggested generalized barrier Lyapunov function on the set $\mathcal{D}_\epsilon \triangleq \{\|x\|_P : \|x\|_P \in [0, \epsilon)\}$, where $\epsilon \in \mathbb{R}+$ is a user-defined constant, is expressed as follows [46].

$$\psi(\|x\|_P) = \frac{\|x\|_P^2}{\epsilon^2 - \|x\|_P^2}. \tag{37}$$

This function is continuously differentiable with the partial derivative

$$\psi_d(\|x\|_P) \triangleq \frac{\text{d}\psi(\|x\|_P)}{\text{d}\|x\|_P^2}, \tag{38}$$

which satisfies

$$2\psi_d(\|x\|_P)\|x\|_P^2 - \psi(\|x\|_P) > 0. \tag{39}$$

Further details and the conditions this function must satisfy can be found in [46].

REFERENCES

[1] J. Kim, H. H. Choi, and J.-W. Jung, "MRAC-based voltage controller for three-phase CVCF inverters to attenuate parameter uncertainties under critical load conditions," *IEEE Transactions on Power Electronics*, vol. 35, no. 1, pp. 1002–1013, 2019.

[2] S. K. Mazumder, A. Kulkarni, S. Sahoo, F. Blaabjerg, H. A. Mantooth, J. C. Balda, Y. Zhao, J. A. Ramos-Ruiz, P. N. Enjeti, P. Kumar *et al.*, "A review of current research trends in power-electronic innovations in cyber–physical systems," *IEEE Journal of Emerging and Selected Topics in Power Electronics*, vol. 9, no. 5, pp. 5146–5163, 2021.

[3] M. Amin, F. F. El-Sousy, G. A. A. Aziz, K. Gaber, and O. A. Mohammed, "CPS attacks mitigation approaches on power electronic systems with security challenges for smart grid applications: A review," *IEEE Access*, vol. 9, pp. 38 571–38 601, 2021.

[4] M. Jamali, M. S. Sadabadi, and A. Oshnoei, "Cyber-resilient adaptive control of grid-following inverter-based resources against measurement manipulation," in *25th IEEE International Conference on Industrial Technology*, 2024, pp. 1–6.

[5] J. K. Singh, S. Prakash, K. Al Jaafari, O. Al Zaabi, K. Al Hosani, R. K. Behera, and U. R. Muduli, "Active disturbance rejection control of photovoltaic three-phase grid following inverters under uncertainty and grid voltage variations," *IEEE Transactions on Power Delivery*, vol. 38, no. 5, pp. 3155–3168, 2023.

[6] R. Errouissi, H. Shareef, and F. Awwad, "Disturbance observer-based control for three-phase grid-tied inverter with LCL filter," *IEEE Transactions on Industry Applications*, vol. 57, no. 5, pp. 5411–5424, 2021.

[7] Y. Zhu and J. Fei, "Disturbance observer-based fuzzy sliding mode control of PV grid-connected inverter," *IEEE Access*, vol. 6, pp. 21 202–21 211, 2018.

[8] A. Benrabah, D. Xu, and Z. Gao, "Active disturbance rejection control of LCL-filtered grid-connected inverter using Padé approximation," *IEEE Transactions on Industry Applications*, vol. 54, no. 6, pp. 6179–6189, 2018.

[9] M. S. Sadabadi, A. Haddadi, H. Karimi, and A. Karimi, "A robust active damping control strategy for an LCL-based grid-connected DG unit," *IEEE Transactions on Industrial Electronics*, vol. 64, no. 10, pp. 8055–8065, 2017.

[10] M. Davari, M. P. Aghababa, F. Blaabjerg, and M. Saif, "An innovative, adaptive faulty signal rectifier along with a switching controller for reliable primary control of GC-VSIs in CPS-based modernized microgrids," *IEEE Transactions on Power Electronics*, vol. 36, no. 7, pp. 8370–8387, 2021.

[11] S. Saha, M. Haque, C. Tan, M. A. Mahmud, M. Arif, S. Lyden, and N. Mendis, "Diagnosis and mitigation of voltage and current sensors malfunctioning in a grid connected PV system," *International Journal of Electrical Power & Energy Systems*, vol. 115, p. 105381, 2020.

[12] S. Y. Gadelovits, Q.-C. Zhong, V. Kadirkamanathan, and A. Kuperman, "Uncertainty and disturbance estimator-based controller equipped with a time-delayed filter to improve the voltage quality of inverters," *IEEE Transactions on Industrial Electronics*, vol. 66, no. 1, pp. 459–469, 2018.

[13] J. S. Costa, A. Lunardi, L. F. N. Lourenço, and A. J. Sguarezi Filho, "Robust predictive repetitive current control for a grid-connected inverter under parametric uncertainty," *IEEE Journal of Emerging and Selected Topics in Power Electronics*, 2023.

[14] X. Liu, L. Feng, X. Kong, S. Guo, and K. Y. Lee, "Tube-based stochastic model predictive control with application to wind energy conversion system," *IEEE Transactions on Control Systems Technology*, vol. 31, no. 5, pp. 2173–2187, 2023.

[15] D. Q. Mayne, S. Raković, R. Findeisen, and F. Allgöwer, "Robust output feedback model predictive control of constrained linear systems: Time varying case," *Automatica*, vol. 45, no. 9, pp. 2082–2087, 2009.

[16] J. Chen, B. Liu, T. Li, and Y. Hu, "Multiplicative attacks with essential stealthiness in sensor and actuator loops against cyber-physical systems," *Sensors*, vol. 23, no. 4, p. 1957, 2023.

[17] Y. Xue and J. M. Guerrero, "Smart inverters for utility and industry applications," in *Proceedings of PCIM Europe 2015; International Exhibition and Conference for Power Electronics, Intelligent Motion, Renewable Energy and Energy Management*. VDE, 2015, pp. 1–8.

[18] B. Ahn, T. Kim, S. Ahmad, S. K. Mazumder, J. Johnson, H. A. Mantooth, and C. Farnell, "An overview of cyber-resilient smart inverters based on practical attack models," *IEEE Transactions on Power Electronics*, 2023.

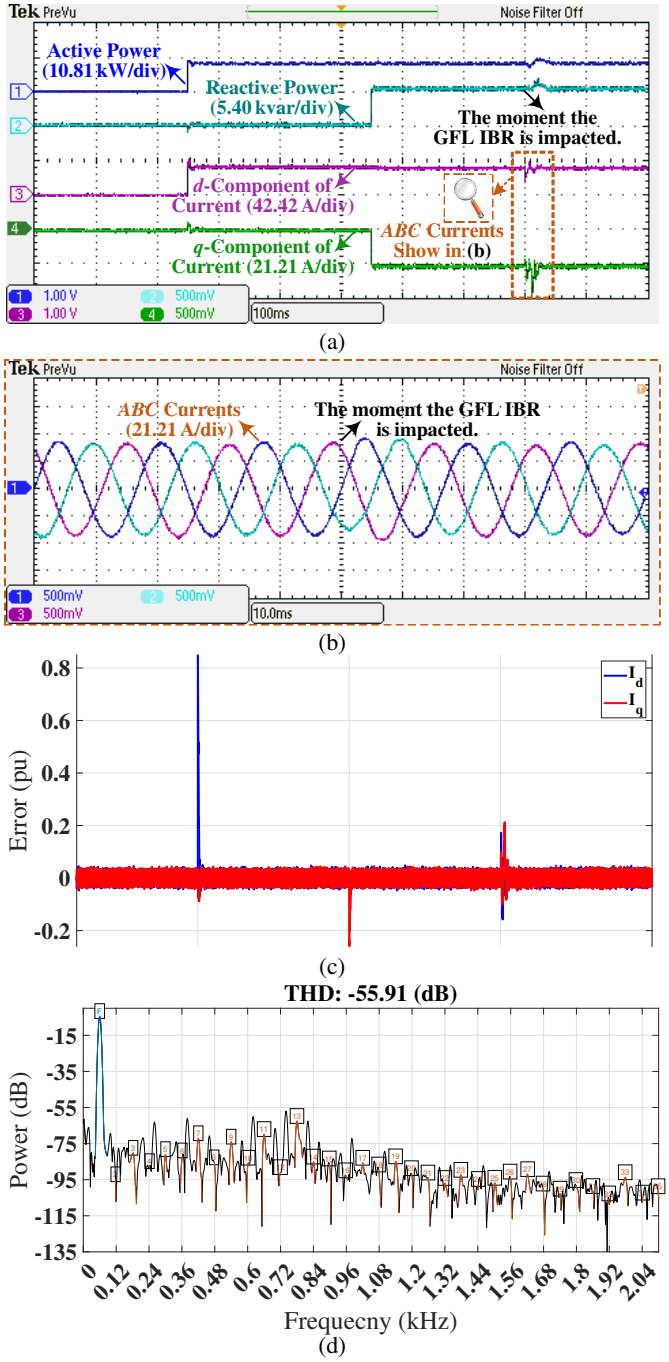

Fig. 12. Experimental results of *Case II*: (a) active and reactive power and the *dq*-frame components of the vector of the current injected to PCC (100 ms/div for the horizontal axis) and (b) the *abc* currents injected to PCC (10 ms/div for the horizontal axis), (c) tracking errors of the *dq*-frame currents, and (d) harmonic spectrum of the three-phase current (for one phase) with a THD of −55.91 dB or, equivalently, 0.16%.

[19] "IEEE guide for cybersecurity of distributed energy resources interconnected with electric power systems," *IEEE Std 1547.3-2023 (Revision of IEEE Std 1547.3-2007)*, pp. 1–183, 2023.

[20] T. D. Do, V. Q. Leu, Y.-S. Choi, H. H. Choi, and J.-W. Jung, "An adaptive voltage control strategy of three-phase inverter for stand-alone distributed generation systems," *IEEE Transactions on Industrial Electronics*, vol. 60, no. 12, pp. 5660–5672, 2012.

[21] F. Blanchini, S. Miani *et al.*, *Set-theoretic methods in control*. Springer, 2008, vol. 78.

[22] M. L. Fravolini and G. Campa, "Design of a neural network adaptive controller via a constrained invariant ellipsoids technique," *IEEE Transactions on Neural Networks*, vol. 22, no. 4, pp. 627–638, 2011.

[23] T. Sadamoto, T. Ishizaki, J.-I. Imura, and T. Kato, "Retrofitting based power system stabilizer design of PV-integrated power systems," in *2018 IEEE Conference on Control Technology and Applications (CCTA)*. IEEE, 2018, pp. 40–45.

[24] D. E. Olivares, A. Mehrizi-Sani, A. H. Etemadi, C. A. Cañizares, R. Iravani, M. Kazerani, A. H. Hajimiragha, O. Gomis-Bellmunt, M. Saeedifard, R. Palma-Behnke, G. A. Jiménez-Estévez, and N. D. Hatziargyriou, "Trends in microgrid control," *IEEE Transactions on Smart Grid*, vol. 5, no. 4, pp. 1905–1919, 2014.

[25] IEEE Standards Coordinating Committee 21, "1547-2018 - IEEE standard for interconnection and interoperability of distributed energy resources with associated electric power systems interfaces," IEEE Std 1547, Tech. Rep., 2018.

[26] S. H. Ali, X. Li, A. S. Kamath, and B. Akin, "A simple plug-in circuit for IGBT gate drivers to monitor device aging: Toward smart gate drivers," *IEEE Power Electronics Magazine*, vol. 5, no. 3, pp. 45–55, 2018.

[27] W. Zhang, D. Xu, P. N. Enjeti, H. Li, J. T. Hawke, and H. S. Krishnamoorthy, "Survey on fault-tolerant techniques for power electronic converters," *IEEE Transactions on Power Electronics*, vol. 29, no. 12, pp. 6319–6331, 2014.

[28] Z. Mao, X.-G. Yan, B. Jiang, and S. K. Spurgeon, "Sliding mode control of nonlinear systems with input distribution uncertainties," *IEEE Transactions on Automatic Control*, vol. 68, no. 10, pp. 6208–6215, 2023.

[29] Z. Zhao, Y. Xu, Y. Li, Y. Zhao, B. Wang, and G. Wen, "Sparse actuator attack detection and identification: A data-driven approach," *IEEE Transactions on Cybernetics*, vol. 53, no. 6, pp. 4054–4064, 2023.

[30] M. Karimi-Ghartemani and H. Karimi, "A robust multivariable approach for current control of voltage-source converters in synchronous frame," *IEEE Journal of Emerging and Selected Topics in Power Electronics*, vol. 9, no. 5, pp. 6174–6183, 2020.

[31] S. A. Khajehoddin, M. Karimi-Ghartemani, and M. Ebrahimi, "Optimal and systematic design of current controller for grid-connected inverters," *IEEE Journal of Emerging and Selected Topics in Power Electronics*, vol. 6, no. 2, pp. 812–824, 2017.

[32] H. K. Khalil, *Nonlinear systems*. 3rd ed. London, U.K.: Prentice-Hall, 2002.

[33] R. A. Horn and C. R. Johnson, *Matrix analysis*, 2nd ed. New York, NY, USA: Cambridge University Press, 2012.

[34] B. Ren, S. S. Ge, K. P. Tee, and T. H. Lee, "Adaptive neural control for output feedback nonlinear systems using a barrier Lyapunov function," *IEEE Transactions on Neural Networks*, vol. 21, no. 8, pp. 1339–1345, 2010.

[35] J. Lofberg, "Yalmip: A toolbox for modeling and optimization in MATLAB," in *2004 IEEE International Conference on Robotics and Automation (IEEE Cat. No. 04CH37508)*. IEEE, 2004, pp. 284–289.

[36] IEEE Std 519-2014 (Revision of IEEE Std 519-1992), "IEEE recommended practice and requirements for harmonic control in electric power systems," IEEE Std 1547, Tech. Rep., 2014.

[37] M. Jamali, M. S. Sadabadi, M. Davari, S. Sahoo, and F. Blaabjerg, "Resilient-by-design control for in situ primary controller of grid-following inverter-based resources by a novel state augmentation to tolerate false data injection cyberattacks," *IEEE Transactions on Power Electronics (Early Access)*, pp. 1–15, 2024.

[38] M. Davari, W. Gao, A. Aghazadeh, F. Blaabjerg, and F. L. Lewis, "An optimal synchronization control method of PLL utilizing adaptive dynamic programming to synchronize inverter-based resources with unbalanced, low-inertia, and very weak grids," *IEEE Transactions on Automation Science and Engineering*, pp. 1–19, 2024.

[39] M. Davari, M. P. Aghababa, F. Blaabjerg, and M. Saif, "A modular adaptive robust nonlinear control for resilient integration of VSIs into emerging modernized microgrids," *IEEE Journal of Emerging and Selected Topics in Power Electronics*, vol. 9, no. 3, pp. 2907–2925, 2021.

[40] A. Aghazadeh, M. Davari, H. Nafisi, and F. Blaabjerg, "Grid integration of a dual two-level voltage-source inverter considering grid impedance and phase-locked loop," *IEEE Journal of Emerging and Selected Topics in Power Electronics*, vol. 9, no. 1, pp. 401–422, 2021.

[41] F. G. Martins, "Tuning PID controllers using the ITAE criterion," *International Journal of Engineering Education*, vol. 21, no. 5, p. 867, 2005.

[42] M. Davari, W. Gao, Z.-P. Jiang, and F. L. Lewis, "An optimal primary frequency control based on adaptive dynamic programming for islanded

modernized microgrids," *IEEE Transactions on Automation Science and Engineering*, vol. 18, no. 3, pp. 1109–1121, 2021.
[43] M. Davari, O. Qasem, W. Gao, , F. Blaabjerg, P. C. Kotsampopoulos, G. Lauss, and N. D. Hatziargyriou, "A reinforcement-learning, optimal approach to in situ power hardware-in-the-loop interface control for testing inverter-based resources: Theory and application of the adaptive dynamic programming based on the hybrid iteration to tackle uncertain dynamics," *IEEE Transactions on Industrial Electronics (Early Access)*, pp. 1–17, 2024, doi: 10.1109/TIE.2024.3426038.
[44] A. Afshari, M. Davari, M. Karrari, W. Gao, and F. Blaabjerg, "A multivariable, adaptive, robust, primary control enforcing predetermined dynamics of interest in islanded microgrids based on grid-forming inverter-based resources," *IEEE Transactions on Automation Science and Engineering*, vol. 21, no. 3, pp. 2494–2506, 2024.
[45] J.-B. Pomet, L. Praly *et al.*, "Adaptive nonlinear regulation: Estimation from the Lyapunov equation," *IEEE Transactions on Automatic Control*, vol. 37, no. 6, pp. 729–740, 1992.
[46] T. Yucelen and J. S. Shamma, "Adaptive architectures for distributed control of modular systems," in *2014 American Control Conference (ACC)*. IEEE, 2014, pp. 1328–1333.

Mahmood Jamali received the B.Sc. degree in Electrical-Control Engineering from Ferdowsi University of Mashhad, Iran, in 2017, and the M.Sc. degree in Control Engineering from Amirkabir University of Technology (Tehran Polytechnic), Iran, in 2020. He is currently pursuing a Ph.D. in Automatic Control and Systems Engineering at the University of Sheffield, United Kingdom. His research interests include advanced control systems and the stability and resilience issues of power electronic converters and modern power grids.

Mahdieh S. Sadabadi (Senior Member, IEEE) is an Assistant Professor at the Department of Electrical and Electronic Engineering at The University of Manchester, Manchester, U.K. Previously, she held academic positions at Queen Mary University of London and the University of Sheffield. She was a Postdoctoral Research Associate at the Department of Engineering, at the University of Cambridge, and a Postdoctoral Fellow in the Division of Automatic Control, Linkoping University in Sweden. She received her Ph.D. in Control Systems from the Swiss Federal Institute of Technology in Lausanne (EPFL), Switzerland in February 2016. Her research focuses on fundamental theoretical and applied research on robust, resilient, secure, and scalable control strategies for cyber-physical systems under uncertainty. Her research is inspired by the control and resilience challenges involved in integrating and interconnection of power electronics converters into future power networks.

Masoud Davari (Senior Member, IEEE) was born in Isfahan, Iran, in 1985. He received the B.Sc. degree (summa cum laude) in electrical engineering (power) from the Isfahan University of Technology, Isfahan, in 2007, the M.Sc. degree (summa cum laude) in electrical engineering (power) from the Amirkabir University of Technology (Tehran Polytechnic), Tehran, Iran, in 2010, and the Ph.D. degree in electrical engineering [power electronics in energy systems (summa cum laude)] from the University of Alberta, Edmonton, AB, Canada, in 2016. He was with Iran's Grid Secure Operation Research Center and Iran's Electric Power Research Institute (EPRI), Tehran, Iran, from January 2010 to December 2011. From April 2015 to June 2017, he was a Senior R & D Specialist and Senior Consultant with Quanta-Technology Company, Markham, ON, Canada, in the field of the dynamic interaction of renewables with smart ac/dc grids and control, protection, and automation of microgrids. In July 2017, he joined as a tenure-track Assistant Professor with the Allen E. Paulson College of Engineering and Computing, Department of Electrical and Computer Engineering, Georgia Southern University (GSU), Statesboro, GA, USA—where he was recommended for being granted "*early*" promotion to Associate Professor and award of "*early*" tenure on December 3, 2021, and officially approved for both on February 16, 2022. He is the Founder and the Director of the Laboratory for Advanced Power and Energy Systems (LAPES) in the state-of-the-art Center for Engineering and Research established in 2021 with GSU—LAPES can be toured online via the https://www.youtube.com/watch?v=mhVHp7uMNKo YouTube link. He has developed and implemented several experimental test rigs for research universities and the power and energy industry. He has also authored several papers published in the IEEE TRANSACTIONS/JOURNAL journals. His research interests include the dynamics, controls, and protections of different power electronic converters utilized in the hybrid ac/dc smart grids and modern power and energy systems testing based on different hardware-in-the-loop (HIL) simulations.

Dr. Davari has been an Associate Editor of the *Elsevier Advances in Electrical Engineering, Electronics and Energy* journal since February 2023. He has been a chapter/clause lead (for Clause #3/Chapter #3) in and an active member of the IEEE Working Group P2004—a newly established IEEE working group entitled "*Recommended Practice for Hardware-in-the-Loop (HIL) Simulation Based Testing of Electric Power Apparatus and Controls*" for the IEEE Standards Association since June 2017. He was a chapter lead in and an active member of the IEEE Power & Energy Society Task Force on "*Innovative Teaching Methods for Modern Power and Energy Systems*" from 2020 to 2024. He was the Chair of the Literature Review Subgroup of DC@Home Standards for the IEEE Standards Association from April 2014 to October 2015. He is an invited reviewer of several of the IEEE TRANSACTIONS/JOURNAL journals, IET journals, *Energies* journals, and various IEEE conferences, the invited speaker at different universities and in diverse societies, and the Best Reviewer of the IEEE TRANSACTIONS ON POWER SYSTEMS in 2018 and 2020. He was an invited member of the Golden Key International Honour Society. He was the recipient of the 2019–2020 Allen E. Paulson College of Engineering and Computing Faculty Award for Outstanding Scholarly Activity in the Allen E. Paulson College of Engineering and Computing at GSU, the Discovery & Innovation Award from the 2020–2021 University Awards of Excellence at GSU, and one of the awardees of the 2021–2022 Impact Area Accelerator Grants (partially funded) at GSU. His biography has been included in *Marquis Who's Who* biographies since 2023. The Awards Committee of the American Society for Engineering Education (ASEE) designated him as the "*finalist*" for the 2024 Curtis W. McGraw Research Award in February 2024. His name was included on *Stanford/Elsevier's Top 2% Scientist Rankings* list in August 2024—thereby identifying and highlighting him as one of the world's leading researchers top-cited in their respective fields—as the list represents approximately 2% of all scientists worldwide.